Final Report for AFRL Contract No. F04700-01-P-0048
Entitled

POWERSAIL
Propulsion System Design Trade Study

By

Lyon B. King
Gordon G. Parker
Martin D. Tervo

Aerophysics, Inc.
30981 Woodbush Road
Calumet, MI 49913

Submitted September 11, 2001

ABSTRACT

The goal of this work was to investigate practical vehicle sizing and performance requirements for a free-flying 500-kW solar array in orbital formation with a power-consuming host vehicle. To meet these requirements, the sail vehicle required independent propulsion for two functions: formation-keeping with host and ACS/Sun-pointing maneuvers. The equations of motion were developed assuming a rigid vehicle subject to gravity, aerodynamic drag, and solar pressure. A numerical optimization tool was developed to select the optimum orbital trajectory for seven canonical electric propulsion technologies: Teflon pulsed plasma thruster (PPT), hydrazine resistojet, hydrazine arcjet, ammonia arcjet, xenon Hall thruster, and xenon ion thruster. Subject to orbital and formation-flying constraints, the optimizer selected the thrust amplitude, thruster firing sequence, and total impulse such that the total vehicle mass was minimized. The best performance (lowest vehicle total mass) was found using a xenon ion propulsion system; the total mass was 1,708 kg for the xenon ion vehicle. The worst performance (highest vehicle total mass) was found using Teflon PPT's; the total mass was 2,367 kg for the PPT vehicle.

Table of Contents

1. Mission Introduction 1

1.1 Mission Identification 1
1.2 Physical Parameter Estimation 1
1.3 Candidate Thruster Technologies 2

2. Dynamic Equations 3

2.1 Q_x Components 3
2.2 Q_y Components 4
2.3 Q_ψ Components 4

3. Equation of Motion Derivation 5

3.1 Gravitational Force .....
3.2 Aerodynamic Drag Force 8
3.3 Solar Pressure 10
3.4 Thrust Forces 10

4. Preliminary Mass Analysis – Continuous Thrust 13

4.1 Assumptions 13
4.2 Sun-pointing 16
4.3 Minimum Drag 17
4.4 Minimum Gravity Gradient 18
4.5 Summary 18

5. Electric Propulsion Trajectory Estimates 21

5.1 Pulse Approximation Based on Throttle-able Results 21
5.2 Optimal Thruster Pulse Generation 21

6. Propulsion System Sizing Calculations 33

6.1 Powersail Thruster Layout 33
6.2 Propulsion System Mass and Power Analysis 33
6.3 Vehicle Performance Summary 35

7. Closing Remarks 37

7.1 Summary 37
7.2 Conclusions 38
7.3 Suggestions for Future Work 39

1. Mission Introduction

The Powersail mission operation regime was specified in the program solicitation and through post-award discussion between Aerophysics, Inc. and AFRL staff. These criteria were used to specify the design space for the proposed vehicle. The purpose of this section is to define mission parameters and introduce assumed physical characteristics of the Powersail vehicle.

1.1 Mission Identification

The overall Powersail mission requirements were defined in Solicitation F04700-01-T-0002 titled, "Powersail – High Power Propulsion System," published in the Commerce Business Daily edition of November 3, 2000. The requirements were brief and open-ended. Specifically, the solicitation stated, "The Powersail High Power Propulsion System is a two-phased program to demonstrate high power (100 kW – 1 MW) capability in space using a deployable, flexible solar-array connected to the host craft using a slack umbilical." This statement encompasses the entire mission definition specified in the program solicitation. Thus, the solicitation effectively stipulated two criteria: 1) solar electric power produced must be between 100 kW and 1 MW, and 2) the Powersail vehicle must have an independent propulsion system allowing the sail to fly in formation with the host vehicle (slack umbilical).

In follow-on conversations with AFRL personnel two other key mission constraints were identified.[1] 1) The target orbit for the Powersail vehicle was chosen as a 900-km circular LEO, and 2) A ten-year mission lifetime was defined. At this altitude, the total mission comprises approximately n=51,030 orbits. To further narrow the open-ended mission definition, Aerophysics investigators have selected a middle-of-the-road target solar energy of 500 kW as the design point.

1.2 Physical Parameter Estimation

As with any conceptual vehicle design analysis, estimation of the Powersail mass properties relied upon assumptions based on existing materials and future predictions. The vehicle mass characteristics used in this study are based largely on performance estimates of the thin-film photovoltaic material which will comprise the bulk of the Powersail.

According to an AFRL presentation by Dr. Troy Meink,[2] the extrapolated far-term performance of the thin-film PV material will likely be

- Specific Power = 400 W/kg
- Energy Efficiency = 15%

With these parameters, and estimating the solar constant $\kappa = 1.4$ kW/m^2, the areal density of the thin-film PV material is $\rho_{film} = 0.53$ kg/m^2. The complete vehicle will require some undetermined structural mass to support and deploy the thin-film blanket. Exact knowledge of the mass properties of the deployed vehicle are impossible to specify at the time of this study. In order to provide an estimate, we have assumed that the required deployment/structural mass will be somewhat less than the mass of the thin-film material. As an arbitrary estimate, we have assumed that the areal density of the entire Powersail vehicle, ρ_{pv}, to be

$$\rho_{pv} \cong 1.75 \times \rho_{film}$$

[1] Telephone conversation with Dr. Frank Gulczinski, AFRL Propulsion Directorate, Edwards AFB, CA, January 2001.

[2] Meink, Troy, "Powersail Program Manager," Air Force Research Laboratory, undated AFRL internal presentation, troy.meink@kirtland.af.mil, 505-846-9331.

Thus, the vehicle areal density assumed for this study is $\rho_{pv} = 0.92$ kg/m^2. We have assumed that the Powersail vehicle mass is uniformly distributed across the surface.

The structural rigidity and other flexible dynamic properties of the Powersail vehicle will be strongly dependent upon the configuration of the support and deployment assembly. Since these properties were not possible to estimate for this initial study, the vehicle was assumed to be rigid in all dynamic simulations.

1.3 Candidate Thruster Technologies

The propulsion system mass necessary to perform a given mission depends upon the thruster technology employed. The investigation reported here was limited to seven canonical electric propulsion (EP) technologies. Numerous studies have established the performance specifications of each technology, namely, specific impulse (I_{sp}), thruster power-specific mass (β_T), power processing unit power-specific mass (β_{PPU}), and power conversion efficiency (η). The thruster operational characteristics assumed in this study are summarized in Table 1-1.

	Teflon PPT	N_2H_4 Resistojet	N_2H_4 Arcjet	NH_3 Arcjet	H_2 Arcjet	Xe Hall	Xe Ion
I_{sp} (sec)	1000	300	500	600	1000	1600	3000
b_T (kg/W)	0.12	0.002	0.0007	0.0007	0.0005	0.003	0.006
b_{ppu} (kg/W)	0.11	0.001	0.0025	0.003	0.0025	0.01	0.01
h	0.07	0.80	0.35	0.36	0.4	0.5	0.65

Table 1-1: Performance characteristics for seven canonical EP technologies investigated for Powersail vehicle sizing estimates.[3]

[3] Martinez-Sanchez, M., and Pollard, J.E., "Spacecraft Electric Propulsion – An Overview," Journal of Propulsion and Power, Vol. 14, No. 5, Sept.-Oct. 1998, pp. 688-699.

2 Dynamic Equations

In this section the dynamic equations of the PowerSail are listed based on the assumptions below with a detailed derivation provided in Section 3.

1. External forces are due to gravity, atmospheric drag, solar pressure, and thrusters.
2. Propulsion system mass is uniformly distributed over the vehicle.
3. The sail is rigid and of uniform density.
4. The sail has only three degrees of freedom (x,y,ψ)
5. The distance between the target spacecraft and the PowerSail, $\sqrt{(x^2+y^2)}$, is sufficiently small such that they enter the earth's shadow at the same time.

The three PowerSail dynamic equations (x,y,ψ respectively) are

$$M\ddot{x} - M(x+r)\dot{\theta}^2 - 2M\dot{\theta}\dot{y} = Q_x \tag{1}$$

$$M\ddot{y} - My\dot{\theta}^2 + 2M\dot{\theta}\dot{x} = Q_y \tag{2}$$

$$\frac{1}{12}ML^2\ddot{\psi} = Q_\psi \tag{3}$$

where M is the sail mass, and L is it's length. Each of the generalized forces, Q_x, Q_y, and Q_ψ can be decomposed into components due to gravity, solar pressure, atmospheric, and the thrusters, that is

$$Q_x = Q_{x,\text{grav}} + Q_{x,\text{aero}} + Q_{x,\text{solar}} + Q_{x,\text{thrust}} \tag{4}$$

$$Q_y = Q_{y,\text{grav}} + Q_{y,\text{aero}} + Q_{y,\text{solar}} + Q_{y,\text{thrust}} \tag{5}$$

$$Q_\psi = Q_{\psi,\text{grav}} + Q_{\psi,\text{aero}} + Q_{\psi,\text{solar}} + Q_{\psi,\text{thrust}} \tag{6}$$

These components, for each of the degrees of freedom are listed below.

2.1 Q_x Components

$$Q_{x,\text{grav}} = -\frac{\mu M}{r^2}\left(1 - \frac{2x}{r}\right) \tag{7}$$

$$\begin{aligned} Q_{x,\text{aero}} &= \left\{\dot{\theta}(y\sin\psi + [r+x]\cos\psi) - \dot{x}\sin\psi + \dot{y}\cos\psi\right\} Z\sin\psi \\ Z &= \frac{\sqrt{2}}{2}A\rho C_d\left|-(\dot{x} - y\dot{\theta})\sin\psi + (\dot{y} + [r+x]\dot{\theta})\cos\psi\right| \end{aligned} \tag{8}$$

$$Q_{x,\text{solar}} = -\left|\cos(\theta+\psi)\right| AP_{\text{solar}}\sin\theta \tag{9}$$

$$Q_{x,\text{thrust}} = -(F_{y1} + F_{y2})\sin\psi + F_x\cos\psi \tag{10}$$

2.2 Q_y Components

$$Q_{y,\text{grav}} = -\frac{\mu M}{r^2}\left(\frac{y}{r}\right) \tag{11}$$

$$\begin{aligned} Q_{y,\text{aero}} &= \left\{-\dot{\theta}\left([r+x]\cos\psi + y\sin\psi\right) + \dot{x}\sin\psi - \dot{y}\cos\psi\right\} Z\cos\psi \\ Z &= \frac{\sqrt{2}}{2} A\rho C_d \left|-(\dot{x} - y\dot{\theta})\sin\psi + (\dot{y} + [r+x]\dot{\theta})\cos\psi\right| \end{aligned} \tag{12}$$

$$Q_{y,\text{solar}} = -\left|\cos\left(\theta+\psi\right)\right| A P_{\text{solar}} \cos\theta \tag{13}$$

$$Q_{y,\text{thrust}} = (F_{y1} + F_{y2})\cos\psi + F_x \sin\psi \tag{14}$$

2.3 Q_ψ Components

$$Q_{\psi,\text{grav}} = -\frac{\mu M}{r^2}\left(\frac{L^2 \sin\psi\cos\psi}{4r}\right) \tag{15}$$

$$Q_{\psi,\text{aero}} = 0 \tag{16}$$

$$Q_{\psi,\text{solar}} = 0 \tag{17}$$

$$Q_{\psi,\text{thrust}} = \frac{L}{2}(F_{y1} - F_{y2}) \tag{18}$$

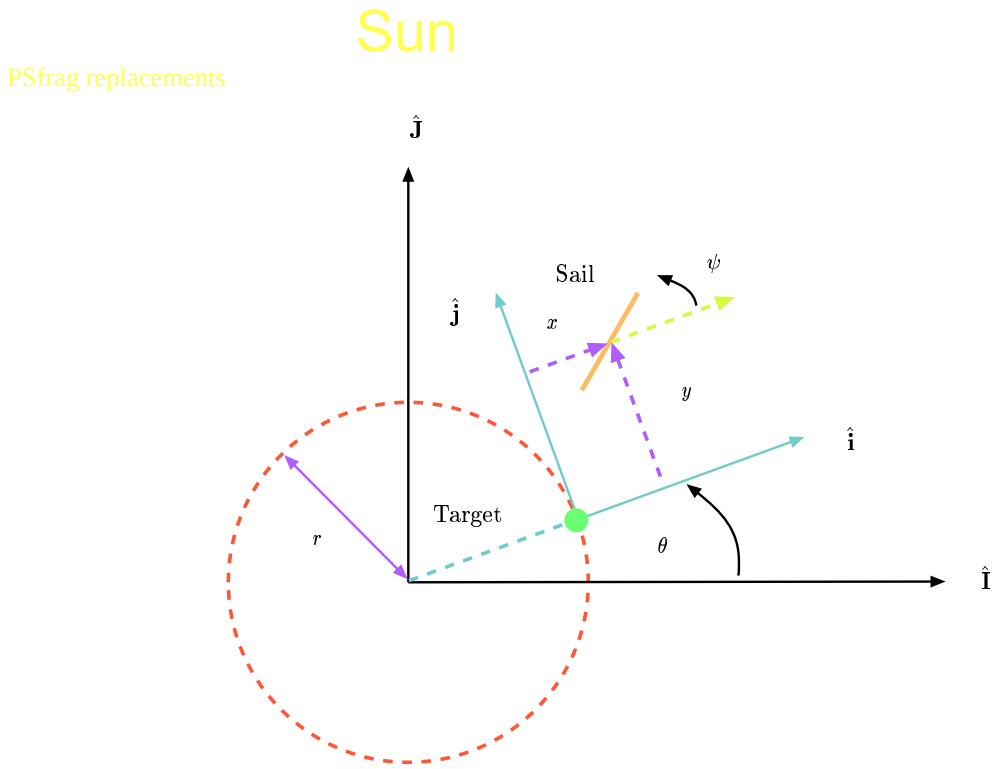

Figure 3-1: Illustration of target and PowerSail degrees of freedom and coordinate frames.

3 Equation of Motion Derivation

Figure 3-1 illustrates the various coordinate frames and degrees of freedom used in the equation of motion development. It is assumed that the orbital plane of both the target (or host) vehicle and the PowerSail contain the sun-pointing vector. Furthermore, the target vehicle has radius r and true anomaly θ. The PowerSail translational degrees of freedom are measured relative to the target vehicle and are x and y. Its single rotational degree of freedom is ψ. The coordinate frames will be denoted using brackets. For example the inertial frame whose center is at the earth's center is denoted $\{\mathrm{I}\}$. Many of the calculations use vector quantities represented in a rotating frame whose center is at the earth's center, but its x-axis tracks the target vehicle. This frame is denoted as $\{1\}$. Finally, a PowerSail body fixed frame is also used to describe locations of thrusters and is denoted $\{\mathrm{b}\}$.

Later in the study a set of 16 thrusters will be described. Eight are used on the outside edges of the sail (4 on each edge for attitude control), 4 are oriented to provide in-plane thrust, and 4 are located at the center for orbit maintenance. Accounting for all 16 thrusters during the dynamic equation derivation over complicates the process. Instead it is assumed that there is thrust capability at the edges of the PowerSail (see Figure 3-2) in the $\hat{\mathbf{x}}_\mathbf{b}$ direction, denoted F_{y1} and F_{y2}. These can be used for either attitude control or, by using simultaneous firings, orbit maintenance. There is also thrust capability in the $\hat{\mathbf{y}}_\mathbf{b}$ direction (in the plane of the PowerSail), denoted F_x. The actual 16 thrusters can be distributed amongst these fundamental thrust magnitudes and directions.

Lagranges equations

$$\frac{d}{dt}\left(\frac{\partial T}{\partial q_i}\right) - \frac{\partial T}{\partial q_i} = Q_i \tag{19}$$

were used to derive Eq. 1 through Eq. 3 where T is the spacecraft kinetic energy, q_i are the generalized coordinates ($q_1 = x$, $q_2 = y$, and $q_3 = \psi$), and Q_i are the generalized forces due to gravity, the atmosphere, solar pressure, and thrusters.

The kinetic energy is,

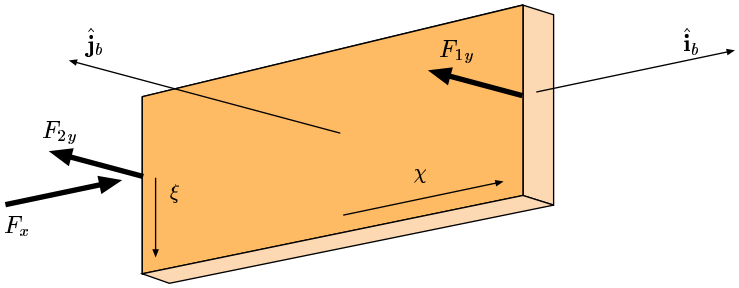

Figure 3-2: Thruster locations, body frame location, and definition of the χ and ξ spatial variables.

$$T = \frac{1}{2} m \int_{-h/2}^{h/2} \int_{-L/2}^{L/2} \mathbf{v}^T \mathbf{v} \, d\chi d\xi \tag{20}$$

where m is the mass per unit area of the spacecraft, h is the height of the sail along its x_b axis, L is the length of the sail along its y_b axis, $\mathbf{v}$ is the absolute velocity of any point along the sail located at (χ, ξ).

The absolute position vector from the origin of the earth centered inertial coordinate system to any point (χ, ξ) on the spacecraft is

$$^1\mathbf{p} = \begin{Bmatrix} r + x + \chi \cos(\psi) \\ y + \chi \sin(\psi) \\ \xi \end{Bmatrix} \tag{21}$$

where the superscript is used to indicate the coordinate frame used to represent any vector. The absolute velocity vector is then

$$^1\mathbf{v} = \begin{Bmatrix} \dot{x} - \chi(\dot{\theta} + \dot{\psi}) \sin(\psi) - y\dot{\theta} \\ \dot{y} + \chi(\dot{\theta} + \dot{\psi}) \cos(\psi) + (r + x)\dot{\theta} \\ 0 \end{Bmatrix} \tag{22}$$

Substituting Eq. 22 into Eq. 20, and noting that odd order terms in χ become zero upon integration, gives

$$\begin{aligned} T &= \frac{1}{2} m \int_{-h/2}^{h/2} \int_{-L/2}^{L/2} \left\{ \left[(r + x)\,\dot{\theta} + \dot{y} \right]^2 + \chi^2 \left(\dot{\psi} + \dot{\theta} \right)^2 \right\} \mathrm{d}\chi \mathrm{d}\xi \\ &= \frac{1}{2} M \left\{ \left[(r + x)\,\dot{\theta} + \dot{y} \right]^2 + \left(\dot{x} - y\dot{\theta} \right)^2 + \frac{1}{12} L^2 \left(\dot{\psi} + \dot{\theta} \right)^2 \right\} \end{aligned} \tag{23}$$

where M is the total mass of the spacecraft, $M = mhL = mA$.

Applying Lagrange's equations to Eq. 23 gives the three dynamic equations for x, y, and ψ,

$$\begin{aligned} &M\ddot{x} - M(x + r)\dot{\theta}^2 - 2M\dot{\theta}\dot{y} = Q_x \\ &M\ddot{y} - My\dot{\theta}^2 + 2M\dot{\theta}\dot{x} = Q_y \\ &\frac{1}{12} ML^2 \ddot{\psi} = Q_\psi \end{aligned} \tag{24}$$

3.1 Gravitational Force – $Q_{i,\text{grav}}$

The virtual work for the gravitational force is

$$\delta W_{\text{grav}} = -\mu m \int_{-h/2}^{h/2} \int_{-L/2}^{L/2} \frac{\mathbf{p}}{|\mathbf{p}|^3} \cdot \delta\mathbf{p} \, d\chi d\xi \tag{25}$$

where μ is the gravitational constant. The absolute position vector, $\mathbf{p}$, represented in the $\{1\}$ frame will be used in the following development. The denominator of Eq. 25 is then

$$\begin{aligned} \left|{}^1\mathbf{p}\right|^3 &= \left[\sqrt{(r+x+\chi\cos\psi)^2+(y+\chi\sin(\psi))^2+\xi^2}\right]^3 \\ &= \left\{r\sqrt{1+\frac{2}{r}(x+\chi\cos\psi)+\frac{1}{r^2}\left[(x+\chi\sin\psi)^2+(y+\chi\sin\psi)^2+\xi^2\right]}\right\}^3 \end{aligned} \tag{26}$$

Assuming that

$$\frac{1}{r^2} \ll 1 \tag{27}$$

the last term of Eq. 26 is neglected, and we can write a simplified version of its reciprocal, for use later in Eq. 25, as

$$\frac{1}{\left|{}^1\mathbf{p}\right|^3} = \frac{1}{r^3}\left[1+\frac{2}{r}(x+\chi\cos\psi)\right]^{-3/2} \tag{28}$$

which can be further simplified using the binomial expansion to give

$$\frac{1}{\left|{}^1\mathbf{p}\right|^3} = \frac{1}{r^3}\left[1-\frac{3}{r}(x+\chi\cos\psi)\right] \tag{29}$$

where again, Eq. 27 has been exploited to neglect higher order terms. To complete Eq. 25 we need to also define $\delta\mathbf{p}$. As stated earlier, we will use a representation of all quantities in the $\{1\}$ frame, resulting in

$$\delta\,{}^1\mathbf{p} = \begin{Bmatrix} \delta x - \chi\sin(\psi)\delta\psi \\ \delta y + \chi\cos(\psi)\delta\psi \\ 0 \end{Bmatrix} \tag{30}$$

Substituting Eq. 29, Eq. 21, and Eq. 30 into Eq. 25 gives the double integral

$$\delta W_{\text{grav}} = -\mu m\int_{-h/2}^{h/2}\int_{-L/2}^{L/2}\frac{1}{r^3}\left[1-\frac{3}{r}(x+\chi\cos\psi)\right]\begin{Bmatrix} r+x+\chi\cos\psi \\ y+\chi\sin\psi \\ \xi \end{Bmatrix}\cdot\begin{Bmatrix} \delta x-\chi\sin(\psi)\delta\psi \\ \delta y+\chi\cos(\psi)\delta\psi \\ 0 \end{Bmatrix}\mathrm{d}\chi\mathrm{d}\xi \tag{31}$$

Evaluating Eq. 31 gives the virtual work expression

$$\begin{aligned} \delta W_{\text{grav}} = -\frac{\mu M}{r^2}\Bigg\{ &\left[1-\frac{2x}{r}-\frac{1}{4r^2}\left(12x^2+L^2\cos(\psi)^2\right)\right]\delta x + \\ &\left[\frac{y}{r}-\frac{1}{4r^2}\left(12xy+L^2\sin\psi\cos\psi\right)\right] \\ &\left[\frac{L^2}{4r}\sin\psi\cos\psi+\frac{L^2}{4r^2}\cos\psi\left(x\sin\psi-y\cos\psi\right)\right]\Bigg\} \end{aligned} \tag{32}$$

Again, higher order terms are neglected consistent with Eq. 27 yielding

$$\delta W_{\text{grav}} = -\frac{\mu M}{r^2}\left\{\left[1-\frac{2x}{r}\right]\delta x+\frac{y}{r}\delta y+\frac{L^2}{4r}\sin\psi\cos\psi\delta\psi\right\} \tag{33}$$

from which we can easily extract the generalized forces due to gravity as

$$Q_{x,\text{grav}} = -\frac{\mu M}{r^2}\left(1-\frac{2x}{r}\right) \tag{34}$$

$$Q_{y,\text{grav}} = -\frac{\mu M y}{r^3} \tag{35}$$

$$Q_{\psi,\text{grav}} = -\frac{\mu M L^2}{4r^3}\left(\sin\psi\cos\psi\right) \tag{36}$$

3.2 Aerodynamic Drag Force – $Q_{i,\text{aero}}$

The aerodynamic pressure, $\mathbf{P}_a$ is assumed to have equal lift ($\mathbf{P}_l$) and drag ($\mathbf{P}_d$) components acting at any point along the spacecraft (χ, ξ),

$$\mathbf{P}_{\text{aero}} = \mathbf{P}_l + \mathbf{P}_d \tag{37}$$

normal to the surface of the spacecraft. Its unit vector, indicating the direction of action of $\mathbf{P}_a$, is

$$\hat{\mathbf{P}}_{\text{aero}} = \hat{\mathbf{i}}_b \times \left(\hat{\mathbf{i}}_b \times \hat{\mathbf{v}}\right) \tag{38}$$

as can be seen from examining Figure 3-2 The quantity $\hat{\mathbf{v}}$ is the unit vector in the direction of the velocity of any point along the spacecraft, $\mathbf{v}(\chi, \xi)$, or

$$\hat{\mathbf{v}} = \frac{\mathbf{v}}{|\mathbf{v}|} \tag{39}$$

The magnitudes of the lift and drag components are

$$P_l = P_d = \frac{1}{2}\rho C_d(\mathbf{v}\cdot\mathbf{v})S_{\text{aero}} \tag{40}$$

where ρ is the density of the atmosphere (assumed constant over the length of the spacecraft), C_d is the drag coefficient, and S_{aero} is the surface area of the spacecraft normal to the velocity,

$$S_{\text{aero}} = A\left|\hat{\mathbf{v}}\cdot\hat{j}_b\right| \tag{41}$$

where A is the total spacecraft area. Using Eq. 40 the magnitude of the total aerodynamic pressure is

$$P_{\text{aero}} = \frac{\sqrt{2}}{2}\rho C_d(\mathbf{v}\cdot\mathbf{v})S_{\text{aero}} \tag{42}$$

and together with Eq. 38, Eq. 41, and Eq. 39 results in the aerodynamic pressure vector

$$\mathbf{P}_{\text{aero}} = \frac{\sqrt{2}}{2}\rho C_d(\mathbf{v}\cdot\mathbf{v})A\left|\frac{\mathbf{v}}{|\mathbf{v}|}\cdot\hat{j}_b\right|\cdot\hat{\mathbf{i}}_b\times\left(\hat{\mathbf{i}}_b\times\frac{\mathbf{v}}{|\mathbf{v}|}\right) \tag{43}$$

Since $|\mathbf{v}|$ is a positive scalar, it can be factored out and cancelled with the term $\mathbf{v}\cdot\mathbf{v}$, resulting in a simpler expression for the pressure vector

$$\mathbf{P}_{\text{aero}} = \frac{\sqrt{2}}{2}\rho C_d A\left|\mathbf{v}\cdot\hat{\mathbf{j}}_b\right|\cdot\hat{\mathbf{i}}_b\times\left(\hat{\mathbf{i}}_b\times\mathbf{v}\right) \tag{44}$$

Using the vector triple product identity a slight improvement in the simplicity of the vector is achieved by noting that

$$\hat{\mathbf{i}}_b\times\left(\hat{\mathbf{i}}_b\times\mathbf{v}\right) = \left(\hat{\mathbf{i}}_b\cdot\mathbf{v}\right)\hat{\mathbf{i}}_b - \mathbf{v} \tag{45}$$

In this form it easily observed that there is no component of the aerodynamic pressure in the $\hat{\mathbf{i}}_b$ direction. Representing these quantities in the $\{1\}$ frame we first note that the $\hat{\mathbf{i}}_b$ vector is

$${}^1\hat{\mathbf{i}}_b = \begin{Bmatrix}\cos\psi\\ \sin\psi\\ 0\end{Bmatrix} \tag{46}$$

which results in

$$ {}^1\hat{\mathbf{i}}_b \times \left({}^1\hat{\mathbf{i}}_b \times {}^1\mathbf{v} \right) = \left\{ \begin{array}{c} \sin\psi \left[-\left(\dot{x} - y\dot{\theta} \right) \sin\psi + \left(\dot{y} + \dot{\theta}\left[r + x \right] \right) \cos\psi \right] \\ \cos\psi \left[\left(\dot{x} - y\dot{\theta} \right) \sin\psi - \left(\dot{y} + \dot{\theta}\left[r + x \right] \right) \cos\psi \right] \end{array} \right\} \tag{47} $$

The virtual work due to the aerodynamic pressure is

$$ \delta W_{\text{aero}} = \int_{-h/2}^{h/2} \int_{-L/2}^{L/2} \mathbf{P}_{\text{aero}} \cdot \delta\mathbf{p} \, d\chi d\xi \tag{48} $$

At this point, we will assume that the aerodynamic pressure is concentrated at the geometric center of the spacecraft. A brief explanation of the motivation for this approximation is given by considering the absolute value term

$$ \left| \mathbf{v} \cdot \hat{\mathbf{j}}_b \right| $$

in the virtual work expression Eq. 48 and Eq. 43. It will be evaluated using all vector quantities represented in the $\{1\}$ frame, that is,

$$ {}^1\hat{\mathbf{j}}_b = \left\{ \begin{array}{c} -\sin\psi \\ \cos\psi \\ 0 \end{array} \right\} \tag{49} $$

Using Eq. 49 and Eq. 22 we have

$$ \left| {}^1\mathbf{v} \cdot {}^1\hat{\mathbf{j}}_b \right| = \chi \left(\dot{\theta} + \dot{\psi} \right) + \left[\dot{y} + (r + x)\, \dot{\theta} \right] \cos\psi - \left(\dot{x} - y\dot{\theta} \right) \sin\psi \tag{50} $$

Since the argument to the absolute value operation changes sign over the range of χ, complications in the integral arise. Specifically, the result will have several conditional statements in the dynamic equations. This problem can be avoided if the net aerodynamic pressure, acting at the spacecraft center of mass, is used instead of a distributed pressure representation. Taking this approach, Eq. 44 becomes

$$ \mathbf{P}_{\text{aero}} = \frac{\sqrt{2}}{2} \rho C_d A \left| \mathbf{v}_{\mathbf{cm}} \cdot \hat{\mathbf{j}}_b \right| \cdot \hat{\mathbf{i}}_b \times \left(\hat{\mathbf{i}}_b \times \mathbf{v}_{\mathbf{cm}} \right) \delta\left(\chi, \xi \right) \tag{51} $$

where the $\delta(\chi, \xi)$ is the Dirac function used to indicate that the pressure is centered at a single point ($\chi = 0, \xi = 0$). The absolute value expression which formerly contained the spatial variable χ becomes

$$ \left| {}^1\mathbf{v}_{\mathbf{cm}} \cdot {}^1\hat{\mathbf{j}}_b \right| = \left[\dot{y} + (r + x)\, \dot{\theta} \right] \cos\psi - \left(\dot{x} - y\dot{\theta} \right) \sin\psi \tag{52} $$

and can be easily moved outside the integral. This term will be denoted as Z for short, that is,

$$ Z \equiv \frac{\sqrt{2}}{2} \rho C_d A \left| {}^1\mathbf{v}_{\mathbf{cm}} \cdot {}^1\hat{\mathbf{j}}_b \right| = \frac{\sqrt{2}}{2} \rho C_d A \left| \left[\dot{y} + (r + x)\, \dot{\theta} \right] \cos\psi - \left(\dot{x} - y\dot{\theta} \right) \sin\psi \right| $$

The virtual work becomes

$$ \delta W_{\text{aero}} = \left\{ \begin{array}{c} \sin\psi \left[-\left(\dot{x} - y\dot{\theta} \right) \sin\psi + \left(\dot{y} + \dot{\theta}\left[r + x \right] \right) \cos\psi \right] \\ \cos\psi \left[\left(\dot{x} - y\dot{\theta} \right) \sin\psi - \left(\dot{y} + \dot{\theta}\left[r + x \right] \right) \cos\psi \right] \end{array} \right\} \cdot \left\{ \begin{array}{c} \delta x - \chi \sin(\psi) \delta\psi \\ \delta y + \chi \cos(\psi) \delta\psi \\ 0 \end{array} \right\} \tag{53} $$

where the double integral has been performed, eliminating the Dirac function, replacing all occurrences of χ with zero. Performing the inner product, and grouping coefficients of the virtual displacements

$$ \begin{aligned} \delta W_{\text{aero}} = Z \Big\{ & \delta x \left[\dot{\theta} \left(y \sin\psi + \left[r + x \right] \cos psi \right) - \dot{x} \sin\psi + \dot{y} \cos\psi \right] \sin\psi + \\ & \delta y \left[-\dot{\theta} \left(y \sin\psi + \left[r + x \right] \cos psi \right) + \dot{x} \sin\psi - \dot{y} \cos\psi \right] \cos\psi \Big\} \end{aligned} \tag{54} $$

from which we can easily extract the generalized forces due to the aerodynamic pressure as

$$Q_{x,\text{aero}} = \left\{ \dot{\theta}(y\sin\psi + [r+x]\cos\psi) - \dot{x}\sin\psi + \dot{y}\cos\psi \right\} Z\sin\psi \tag{55}$$

$$Q_{y,\text{aero}} = \left\{ -\dot{\theta}\left([r+x]\cos\psi + y\sin\psi\right) + \dot{x}\sin\psi - \dot{y}\cos\psi \right\} Z\cos\psi \tag{56}$$

$$Q_{\psi,\text{aero}} = 0 \tag{57}$$

3.3 Solar Pressure – $Q_{i,\text{solar}}$

The solar pressure acts in the negative $\hat{\mathbf{J}}$ direction

$$^{I}\mathbf{P}_{\text{solar}} = \left\{ \begin{array}{c} 0 \\ -P_{\text{solar}} \\ 0 \end{array} \right\} \tag{58}$$

or represented in the $\{1\}$ frame

$$^{1}\mathbf{P}_{\text{solar}} = \left\{ \begin{array}{c} -P_{\text{solar}}\sin\theta \\ -P_{\text{solar}}\cos\theta \\ 0 \end{array} \right\} \tag{59}$$

and acts on the sail area incident with the inertial sun direction ($\hat{J}$). This fractional area can be found by forming the dot product of the spacecraft fixed $\hat{\mathbf{y}}_b$ body axis with the inertial $\hat{\mathbf{J}}$ unit vector. The solar pressure incident area is then the product of the total area A and the absolute value of the fractional area S_{solar} indicating that the solar pressure applies to either side of the sail. Performing this operation using quantities represented in the $\{\text{I}\}$ frame yields

$$S_{\text{solar}} = A\left| {}^{I}\mathbf{y}_b \cdot \hat{\mathbf{J}} \right| = A\left| \left\{ \begin{array}{c} -\sin(\theta+\psi) \\ \cos(\theta+\psi) \\ 0 \end{array} \right\} \cdot \hat{\mathbf{J}} \right| = A\left|\cos(\theta+\psi)\right| \tag{60}$$

The virtual work due to solar pressure is formed in the usual manner, representing all quantities in the $\{1\}$ frame

$$\delta W_{\text{solar}} = S_{\text{solar}} \int_{-h/2}^{h/2} \int_{-L/2}^{L/2} {}^{1}\mathbf{P}_{\text{solar}} \cdot \delta^{1}\mathbf{p}\, d\chi d\xi \tag{61}$$

where the virtual displacement is given by Eq. 30 and the solar pressure is from Eq. 59. Integrating Eq. 61 gives

$$\delta W_{\text{solar}} = -\left|\cos(\theta+\psi)\right| AP_{\text{solar}} \left\{\sin\theta\delta x + \cos\theta\delta y\right\} \tag{62}$$

The solar pressure force components in the r and θ directions are easily extracted from Eq. 62 as the coefficients of δx and δy respectively, that is,

$$Q_{x,\text{solar}} = -AP_{\text{solar}}\left|\cos(\theta+\psi)\right|\sin\theta \tag{63}$$

$$Q_{y,\text{solar}} = -AP_{\text{solar}}\left|\cos(\theta+\psi)\right|\cos\theta \tag{64}$$

$$Q_{\psi,\text{solar}} = 0 \tag{65}$$

3.4 Thrust Forces – $Q_{i,\text{thrust}}$

The PowerSail spacecraft is assumed to have 3 bidirectional thrusters, 2 are in body fixed y direction (out of the plane of the sail) and 1 is in the body fixed x direction (in the plane of the sail). One y-axis thruster is located along the x-axis at a distance of $L/2$ from the center of mass. The second y-axis thruster is also along the x-axis, but at a distance of $-L/2$ from the center of mass. The x-axis thruster is collocated with the first y-axis thruster. In the following sections, the thruster force vectors, and virtual displacement vectors are derived and used to generate the virtual work of each thruster.

3.4.1 Y-Axis Thruster 1

The thrust vector is simply

$$ {}^1\mathbf{F}_{y_1} = \begin{Bmatrix} -F_{y_1} \sin\psi \\ F_{y_1} \cos\psi \\ 0 \end{Bmatrix} \tag{66} $$

The virtual displacement is found from Eq. 30 by setting $\chi = L/2$, that is

$$ \delta {}^1\mathbf{P}_{F_{y_1}} = \delta {}^1\mathbf{p} \Big|_{\chi=\frac{L}{2}} = \begin{Bmatrix} \delta x - \frac{L}{2} \sin\psi \delta\psi \\ \delta y + \frac{L}{2} \cos\psi \delta\psi \\ 0 \end{Bmatrix} \tag{67} $$

The virtual work of the thruster is then

$$ \begin{aligned} \delta W_{F_{y_1}} &= {}^1\mathbf{F}_{y_1} \cdot \delta {}^1\mathbf{P}_{F_{y_1}} \\ &= -F_{y_1} \sin\psi \delta x + F_{y_1} \cos\psi \delta y + \frac{L}{2} F_{y_1} \delta\psi \end{aligned} \tag{68} $$

3.4.2 Y-Axis Thruster 2

The thrust vector is simply

$$ {}^1\mathbf{F}_{y_2} = \begin{Bmatrix} -F_{y_2} \sin\psi \\ F_{y_2} \cos\psi \\ 0 \end{Bmatrix} \tag{69} $$

The virtual displacement is found from Eq. 30 by setting $\chi = -L/2$, that is

$$ \delta {}^1\mathbf{P}_{F_{y_2}} = \delta {}^1\mathbf{p} \Big|_{\chi=-\frac{L}{2}} = \begin{Bmatrix} \delta x + \frac{L}{2} \sin\psi \delta\psi \\ \delta y - \frac{L}{2} \cos\psi \delta\psi \\ 0 \end{Bmatrix} \tag{70} $$

The virtual work of the thruster is then

$$ \begin{aligned} \delta W_{F_{y_2}} &= {}^1\mathbf{F}_{y_2} \cdot \delta {}^1\mathbf{P}_{F_{y_2}} \\ &= -F_{y_2} \sin\psi \delta x + F_{y_2} \cos\psi \delta y - \frac{L}{2} F_{y_2} \delta\psi \end{aligned} \tag{71} $$

3.4.3 X-Axis Thruster

The thrust vector is simply

$$ {}^1\mathbf{F}_{x} = \begin{Bmatrix} F_x \cos\psi \\ F_x \sin\psi \\ 0 \end{Bmatrix} \tag{72} $$

Since this thruster is located at the same place as the Y-axis thruster one, the virtual displacement is the same as Eq. 67 resulting in the virtual work

$$ \delta W_{F_x} = F_x \cos\psi \delta x + F_x \sin\psi \delta y \tag{73} $$

3.4.4 Combined Thrust Force

The net force of all three thrusters is found by summing the coefficients of the virtual displacements from Eq. 68, Eq. 71, and Eq. 73, that is

$$Q_{x,\text{thrust}} = -\left(F_{y1} + F_{y2}\right)\sin\psi + F_x\cos\psi \tag{74}$$

$$Q_{\theta,\text{thrust}} = \left(F_{y1} + F_{y2}\right) + F_x\sin\psi \tag{75}$$

$$Q_{\psi,\text{thrust}} = \frac{L}{2}\left(F_{y1} - F_{y2}\right) \tag{76}$$

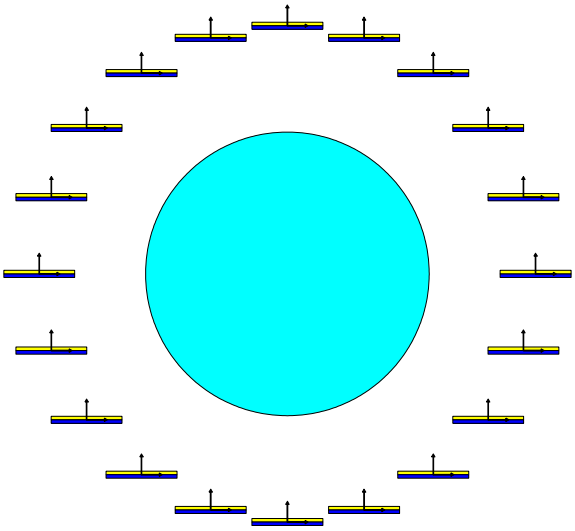

Figure 4-1: Sun pointing orientation.

Description	Symbol	Units	Value
Orbital period	τ	sec	6180
Orbital radius	r	m	7,277,759
Atmospheric density	ρ	kg/m^3	5.76E-15
Drag coefficient	C_d	n.d.	2.0
Nominal solar pressure	P_o	N/m^2	4.667E-6
Total number of orbits	n	n.d.	51030

Table 4-1: Mission specific parameters.

4 Preliminary Mass Analysis – Continuous Thrust

This section investigates three different spacecraft orientation scenarios where the three thrusters are assumed to be throttle-able. This will lend insight into the case where the thrusters have fixed amplitude, addressed in Section 5.

The first orientation, called sun pointing, keeps the spacecraft oriented such that the solar power absorption material is always pointing directly at the sun as shown in Figure 4-1. The second orientation, called minimum drag, keeps the spacecraft oriented such that the sail never encounters atmospheric drag (neglecting shear) and is shown in Figure 4-2. The third configuration, called minimum gravity gradient, results in no gravity gradient torques and is shown in Figure 4-3.
For each orientation the three thruster force histories are computed analytically and compared.

4.1 Assumptions

In addition to the assumptions employed during the equation of motion development, mission specific assumptions are listed in Table 4-1. Thruster and solar sail constants are listed in Table 4-2. As a canonical case, a thruster $I_{sp} = 1000$ seconds (representative of an H_2 arcjet or PPT) was chosen.

Finally, the PowerSail is assumed to be sufficiently close to the host such that both the host and PowerSail enter (and exit) the earth's shadow at the same time, or more generally, that their true anomalies are equal. The angle α

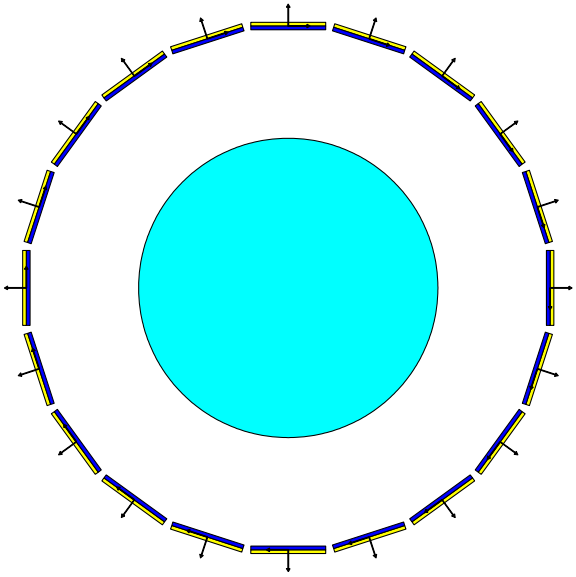

Figure 4-2: Minimum drag orientation.

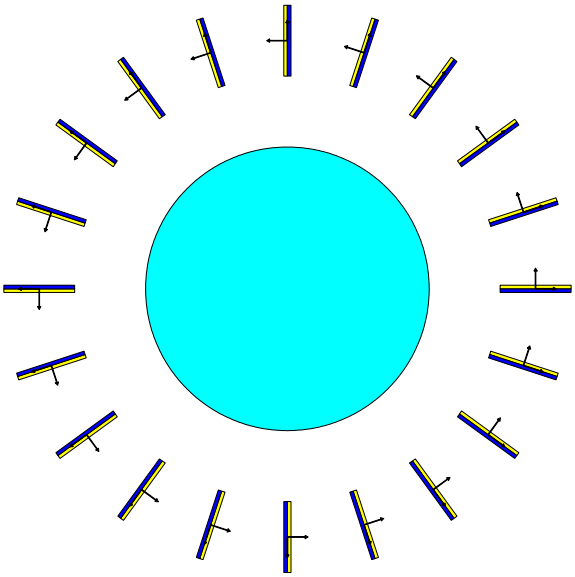

Figure 4-3: Minimum gravity gradient orientation.

Description	Symbol	Units	Value
Thruster specific impulse	I_{sp}	sec	1000
Solar power density	K_{pv}	W/m^2	1400
Sail areal mass	ρ_{pv}	kg/m^2	0.92
Sail efficiency	ϵ_{pv}	n.d.	0.15

Table 4-2: Thruster and sail parameters.

PStrag replacements

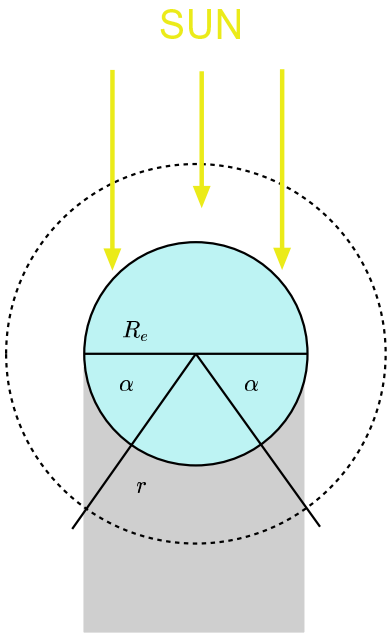

Figure 4-4: Geometry of earth's shadow.

$$\alpha = \cos^{-1}(Re/r) = 28.835^\circ \tag{77}$$

will be used to define the earth shadow as shown in Fig 4-4. The solar pressure is modeled with a step discontinuity at the shadow transitions, and is defined as

$$P_{\text{solar}} = \begin{cases} 0 & : \quad \pi + \alpha \leq \theta \leq -\alpha \\ P_o & : \quad \pi + \alpha > \theta > -\alpha \end{cases} \tag{78}$$

The mission requirement of P_o watts is translated into an average energy per orbit, denoted E_o, and is ,

$$E_o = \frac{1}{2}\tau P_o = \frac{1}{2}(6180)(500,000) = 1,545\text{MJ}$$

This can also be related to the solar sail energy absorption properties, and an effective pointing angle, γ

$$E_o = \frac{AK_{\text{pv}}\epsilon_{\text{pv}}\gamma}{\dot{\theta}} \tag{79}$$

which will be used to determine the sail area, A, for each orientation using an analytical expression for γ.

The mass of the vehicle will be denoted M and for this analysis consists of only the mass of the sail (including support structure), and the fuel. For each case, this will be denoted

$$M = m_{\text{sail}} + m_{\text{fuel}}$$

The mass of the sail is simply the product of the area and the effective area density,

$$m_{\text{sail}} = A\rho_{pv}$$

The mass of the fuel is

$$m_{\text{fuel}} = \frac{n\sum\left|\hat{F}\right|}{gI_{sp}} \tag{80}$$

where $\sum\left|\hat{F}\right|$ is the total thruster impulse per orbit.

4.2 Sun Pointing

The sun pointing trajectory of Figure 4-1, is defined by

$$\begin{aligned} x &= \dot{x} = \ddot{x} = 0 \\ y &= \dot{y} = \ddot{y} = 0 \\ \psi &= -\theta \\ \dot{\psi} &= -\dot{\theta} \\ \ddot{\psi} &= \ddot{\theta} = 0 \end{aligned} \tag{81}$$

Applying these conditions to the dynamic equations of Eq. 1 through Eq. 3 gives

$$\begin{aligned} (F_{y1}+F_{y2})\sin\theta + F_x\cos\theta &= \frac{\sqrt{2}}{2}A\rho C_d r^2\dot{\theta}^2\left|cos\theta\right|\sin\theta\cos\theta + AP_{\text{soloar}}\sin theta \\ (F_{y1}+F_{y2})\cos\theta - F_x\sin\theta &= \frac{\sqrt{2}}{2}A\rho C_d r^2\dot{\theta}^2\left|cos\theta\right|\cos\theta^2 + AP_{\text{soloar}}\cos theta \\ \frac{L}{2}(F_{y1}-F_{y2}) &= \frac{\mu M}{4r^3}L^2\sin\theta\cos\theta \end{aligned} \tag{82}$$

Solving these for the three forces yields force time histories that maintain the PowerSail as shown in Fig 4-1, that is

$$\begin{aligned} F_{y1} &= \frac{\sqrt{2}}{4}A\rho C_d r^2\dot{\theta}^2\left|cos\theta\right|\cos\theta + \frac{1}{2}AP_{\text{soloar}} - \frac{\mu M}{4r^3}L\sin\theta\cos\theta \\ F_{y2} &= \frac{\sqrt{2}}{4}A\rho C_d r^2\dot{\theta}^2\left|cos\theta\right|\cos\theta + \frac{1}{2}AP_{\text{soloar}} + \frac{\mu M}{4r^3}L\sin\theta\cos\theta \\ F_x &= 0 \end{aligned} \tag{83}$$

The effective pointing angle, γ_{sp}, is

$$\gamma_{sp} = \int_{\theta_1}^{\theta_2} d\theta$$

where for this case $\theta_1 = -\alpha$ and $\theta_2 = \pi + \alpha$. Solving the integral gives

$$\gamma_{sp} = \pi + 2\alpha = 4.1481$$

The sail area can then be computed using Eq. 79 and the values of Table 4-2 as

$$A_{sp} = \frac{E_o\dot{\theta}}{K_{pv}\epsilon_{pv}\gamma_{sp}} = 1803m^2$$

Assuming a sail material (with structure) area density as given in Table 4-2, the mass of the sail, not including propellant, is

$$m_{sp,\text{sail}} = A_{sp}\rho_{pv} = 1659kg$$

The mass of the fuel is not readily computed using Eq. 80 since the mass of the PowerSail is needed to compute the thruster forces, and the impulse $\hat{F}$. Instead, the fuel mass was calculated by iterating the force equations on the total mass M until the required fuel mass equaled the difference between the total mass, and $m_{sp,\text{sail}}$. In this way the fuel mass was found to be

$$m_{sp,\text{fuel}} = 510kg$$

The time histories of the force profiles are shown in Figure 4-5 through Figure 4-7 using the blue lines.

4.3 Minimum Drag

The minimum drag trajectory of Figure 4-2 is defined by

$$\begin{aligned} x &= \dot{x} = \ddot{x} = 0 \\ y &= \dot{y} = \ddot{y} = 0 \\ \psi &= -\frac{\pi}{2} \\ \dot{\psi} &= \ddot{\psi} = 0 \end{aligned} \tag{84}$$

Applying these conditions to the dynamic equations of Eq. 1 through Eq. 3 gives

$$\begin{aligned} F_{y1} + F_{y2} &= -AP_{\text{solar}} \sin\theta \left|\cos\left(\theta - \frac{\pi}{2}\right)\right| \\ F_x &= AP_{\text{solar}} \cos\theta \left|\cos\left(\theta - \frac{\pi}{2}\right)\right| \\ 0 &= \frac{L}{2}(F_{y1} - F_{y2}) \end{aligned} \tag{85}$$

Solving these for the three forces yields the thruster histories that maintain the PowerSail as shown in Fig 4-2, that is

$$\begin{aligned} F_{y1} = F_{y2} &= -\frac{1}{2} AP_{\text{solar}} \sin\theta \left|\sin\theta\right| \\ F_x &= AP_{\text{solar}} \cos\theta \left|\sin\theta\right| \end{aligned} \tag{86}$$

The effective pointing angle, γ_{md}, is

$$\gamma_{md} = \int_{\theta_1}^{\theta_2} \sin\theta \, d\theta$$

where for this case $\theta_1 = 0$ and $\theta_2 = \pi$. Solving the integral gives

$$\gamma_{sp} = 2$$

The sail area can then be computed using Eq. 79 and the values Table 4-2 as

$$A_{md} = \frac{E_o \dot{\theta}}{K_{pv} \epsilon_{pv} \gamma_{md}} = 3740m^2$$

Assuming a sail material (with structure) area density as given in Table 4-2, the mass of the sail, not including propellant, is

$$m_{md,\text{sail}} = A_{md} \rho_{pv} = 3441kg$$

Unlike the sun pointing case, for minimum drag the force balance of Eq. 86 does not depend on the sail mass. Therefore, the fuel is computed directly from Eq. 80.

$$m_{md,\text{fuel}} = 258kg$$

The time histories of the forces are shown in Figure 4-5 through Figure 4-7 using the red lines.

4.4 Minimum Gravity Gradient

The minimum gravity gradient trajectory is defined by

$$\begin{aligned} x &= \dot{x} = \ddot{x} = 0 \\ y &= \dot{y} = \ddot{y} = 0 \\ \psi &= \dot{\psi} = \ddot{\psi} = 0 \end{aligned} \tag{87}$$

Applying these conditions to the dynamic equations of Eq. 1 through Eq. 3 gives

$$\begin{aligned} F_{y1} = F_{y2} &= \frac{1}{2} A P_{\text{solar}} \cos\theta \left|\cos\theta\right| + \frac{\sqrt{2}}{4} A \rho C_d r^2 \dot{\theta}^2 \\ F_x &= A P_{\text{solar}} \sin\theta \left|\cos\theta\right| \end{aligned} \tag{88}$$

which yields the thruster histories that maintain the PowerSail as shown in Fig 4-3.

The effective pointing angle, γ_{mg}, is

$$\gamma_{mg} = \int_{\theta_1}^{\theta_2} \cos\theta \; d\theta$$

where for this case $\theta_1 = -\alpha$ and $\theta_2 = 0$. Solving the integral gives

$$\gamma_{mg} = 1 + \sin\alpha = 1.4823$$

The sail area can then be computed using Eq. 79and the values of Table 4-2 as

$$A_{mg} = \frac{E_o \dot{\theta}}{K_{pv} \epsilon_{pv} \gamma_{mg}} = 5047 m^2$$

Assuming a sail material (with structure) area density as given in Table 4-2, the mass of the sail, not including propellant, is

$$m_{mg,\text{sail}} = A_{mg} \rho_{pv} = 4643 kg$$

Just like the minimum drag case, the fuel is computed directly from Eq. 80 as

$$m_{mg,\text{fuel}} = 479 kg$$

The time histories of the force profiles are shown in Figure 4-5 through Figure 4-7 using the black lines.

4.5 Summary

Table 4-3 summarizes the results of the previous sections, including extracting the total impulse from the plots of Figure 4-5 through Figure 4-7. For the 6180 second period orbit considered (approximately 900 kilometer altitude), it is clear that a sun pointing configuration has the smallest area, and smallest total mass. It should be noted that for lower orbits the atmospheric drag term in the sun pointing equations will eventually dominate. When this occurs the minimum drag orientation will become the lower mass solution. There are two entries for the sun pointing case using different E_o requirements. The second one has an E_o that is 5% lower than the rest. This will be used for comparison and discussion with the fuel optimal results of Section 5.2. It should be noted that the force profiles as summarized in Figure 4-5 through Figure 4-7, ensure zero sail/host formation error throughout the orbit.

Although the analysis for the mission with continually throttle-able thrusters is fairly straightforward, this is not the case when using electric propulsion thrusters having fixed amplitudes as considered in the next section.

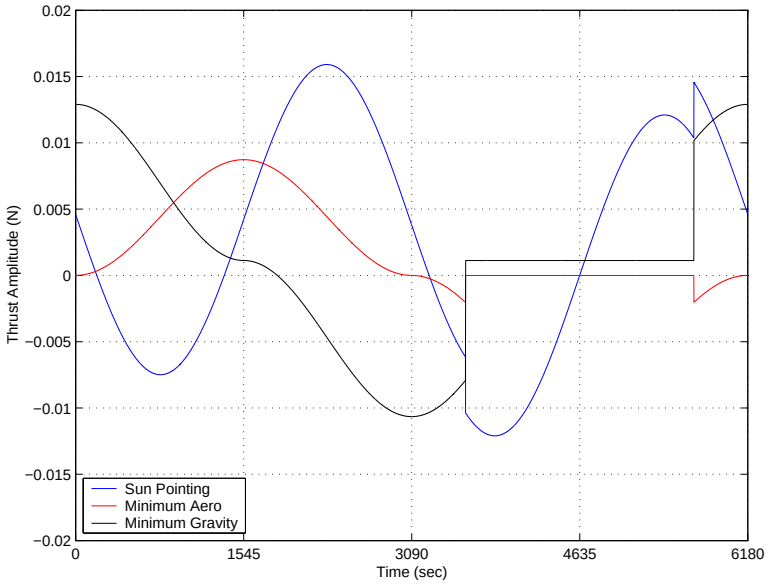

Figure 4-5: Time history of the F_{y1} thruster.

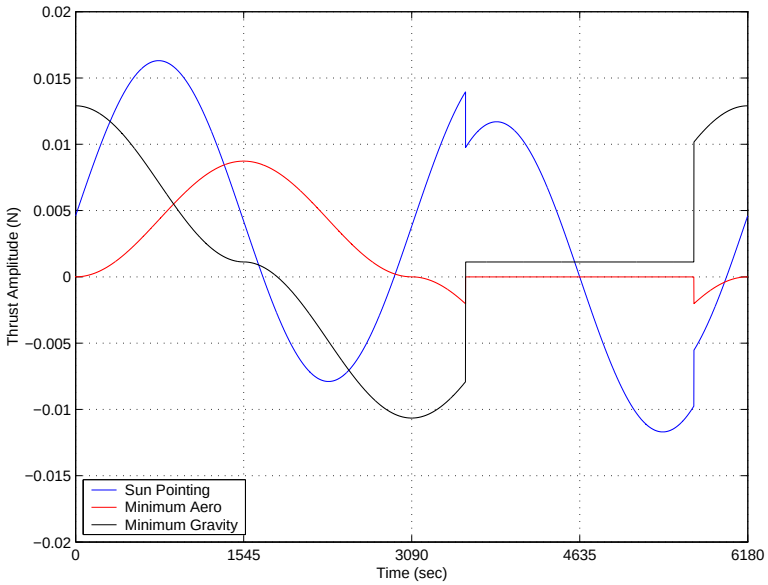

Figure 4-6: Time history of the F_{y2} thruster.

Traj. Name	Length (m)	Area (m^2)	m_{sail} (kg)	m_{fuel} (kg)	m_{total} (kg)	Impulse (N-s)	Ptg. Time (sec)	Energy/Orbit (MJ)
Sun Ptg	42.46	1803	1659	510	2169	98	4080	1,545
Sun Ptg	41.40	1713	1576	471	2047	91	4080	1,468
Min Drag	61.16	3741	3441	258	3699	50	1967	1,545
Min Grav	71.04	5047	4643	479	5122	92	1458	1,545

Table 4-3: Summary of mass and impulse results for the three different PowerSail trajectory orientations.

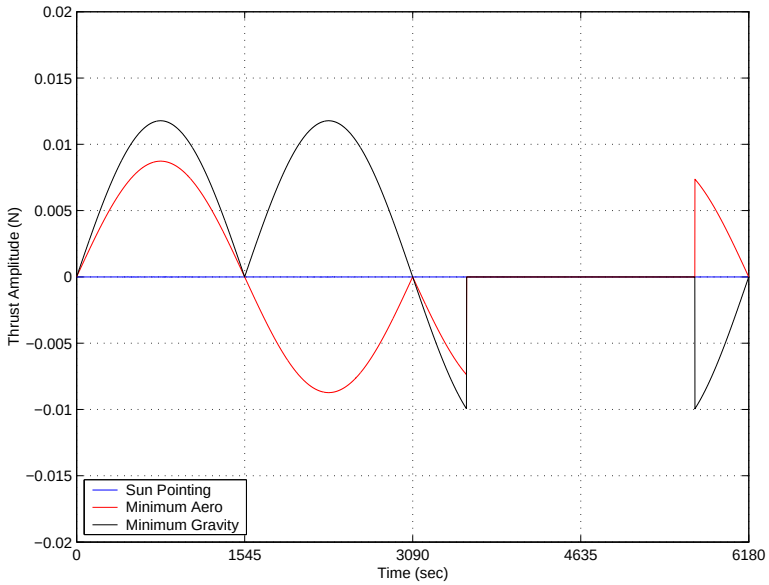

Figure 4-7: Time history of the F_x thruster.

5 Electric Propulsion Trajectory Estimates

Several different propulsion technologies are available for use on the PowerSail (e.g. teflon PPT, hydrazine arcjet, and xenon ion). Although some EP systems allow limited throttling, this study conservatively assumed that the thrusters were capable of only discrete thrust amplitudes. Since the goal of this study was to determine the PowerSail configuration (size and thruster technology) with smallest total mass, it was necessary to determine the fuel requirements for various thruster technologies. In addition the PowerSail was to satisfy power and station keeping requirements. That is, the PowerSail must return to its starting position and orientation after one orbit.

A simple approach would be to use the information learned from Section 4 using PowerSail configurations and their throttle-able thrust profiles to set the pulse amplitudes and durations. Unfortunately, this leads to large PowerSail pointing inaccuracies effecting both power generation and station keeping as will be shown in Section 5.1.

Another approach is to use a numerical optimization code to determine the thrust durations and PowerSail size such that the system mass is minimized while ensuring that power generation and station keeping constraints are satisfied. This has the added benefit of generating optimal PowerSail trajectories, different from the ones shown in the throttle-able section. This method is described in detail in Section 5.2 where it is shown that the best PowerSail trajectory is somewhere between the sun pointing and aero optimal described earlier. This allows the PowerSail system mass to be less than that of the throttle-able solution by trading off pointing accuracy for fuel mass.

5.1 Pulse Approximation Based on Throttle-able Results

Using the results of Figure 4-5 through Figure 4-7 an approximate pulse profile was constructed as shown in Figure 5-3. The goal of this profile was to exploit the benefit of true sun-pointing to reduce vehicle mass. The amplitudes and pulse durations were selected by decomposing the throttle-able thrust profile into a constant thrust portion (zero moment), and the moment producing portion as shown, for F_{y1}, in Figure 5-1.

The constant thrust portion was approximated as having an amplitude of 4.6 mN between 0 and 3585 seconds, and again between 5685 seconds to the end of the maneuver. After applying this approximation to the throttle-able solution, constant amplitude pulses were selected to generate an average amplitude. The decomposition of the approximate pulse profile is shown in Figure 5-2.

The resulting approximate pulse profiles are shown in Figure 5-3 for all three thrusters. They use more impulse, and thus result in larger PowerSail system mass, as compared to the true sun pointing solution of the previous section. However, they represent a reasonable first cut.

The dynamic simulation of the PowerSail was run using the pulse profiles described above, with the resulting trajectories shown in Figure5-4. The system mass was fixed to be the same as the throttle-able solution of 2169 kg. It is clear that the approximations lead to significant power generation and station keeping errors after one orbit.

Due to the severity of the pointing and station keeping errors associated with approximate thrust profiles, it was decided that they would not be sufficient for determining meaningful system mass estimates. Furthermore, it is not readily apparent how the profiles should be modified to improve performance. Instead an optimization capability was developed that generates pulse profiles that achieve the mission requirements, while minimizing system mass.

5.2 Optimal Thruster Pulse Generation

Each y-axis thruster (F_{y1} and F_{y2}) was allowed to have two positive and two negative pulses, all of the same amplitude. In addition, a center thruster was allowed to have a different amplitude and two positive pulses. Finally, the x-axis thruster was allowed to have its own amplitude, and again, two positive and two negative firings. The optimization code was allowed to select all the amplitudes and thrust times. The pulses were allowed to overlap, mimicking the effect of two thrusters firing simultaneously to double the force. In addition, it could give the PowerSail an initial orientation and angular rate. Finally, the PowerSail was assumed to be square with the length of it being a free parameter.

Constraints were imposed on both the power generation and station keeping requirements. Specifically, the energy per orbit was required to be within 5% of the previously computed value of 1,545MJ and the PowerSail was required to return to the starting position and orientation after one orbit, to within 1 centimeter, and 0.1 degrees orientation. The cost function, J,

$$J = m_{sys} \tag{89}$$

Thruster Technology	Impulse Per Orbit (Ns)	Center Thruster Amplitude (N)	Outboard Thruster Amplitudes (N)	In-Plane Thruster Amplitude (N)	Sail Length (m)	Effective Pointing Time (sec)
Teflon PPT	37.64	3814.0	18.0	452.3	41.92	3978.1
N_2H_4 Resistojet	33.53	7157.2	1896.6	48.8	41.83	3994.8
N_2H_4 Arcjet	36.67	7604.2	19.5	1003.8	41.91	3979.0
NH_3 Arcjet	33.22	9005.4	14.6	121.0	41.90	3981.6
H_2 Arcjet	37.59	7892.0	766.7	925.0	41.92	3978.3
Xe Hall	40.91	10845.0	21.8	101.3	41.89	3982.8
Xe Ion	36.32	10532.0	66.7	210.4	41.89	3984.0

Table 5-1: Impulse and thrust requirements from the mass optimization results.

was simply the total mass of the system, including the sail mass, fuel mass, and inert thruster mass (for derivation of fuel and inert mass see Section 6).

$$m_{sys} = A\rho_{pv} + \frac{n}{I_{sp}g}\sum \hat{F} + \frac{\beta g I_{sp}}{\eta}\left(8F_{y,amp} + 4F_{x,amp} + 4F_{c,amp}\right)$$

where ρ_{pv} is the PowerSail areal density, n is the total number of orbits during the PowerSail lifetime, $F_{y,amp}$ is the amplitude of the y-axis (outboard) thrusters, $F_{x,amp}$ is the amplitude of the x-axis (in-plane) thrusters, $F_{c,amp}$ is the amplitude of the center thruster, and $\hat{F}$ is the total impulse for one orbit.

Instead of writing a custom optimization code, MATLAB's constrained optimization algorithm was used. It relies on the standard Sequential Quadratic Programming approach as described in the MATLAB manuals. It should be noted that all the results here, while being mass extremum solutions, are not claimed to be globally optimal. Unfortunately, the system is sufficiently complex that a formal proof of global optimality is impossible.

The seven thruster technologies, listed in Table 1-1, were used to determine the mass optimal results of Figure 5-5 through Figure 5-11. The x and y quantities in the (b) plots are the same as those of Eq. 1 through Eq. 3. The inertial PowerSail orientation angle, Ψ is related to ψ and θ by

$$\Psi = \psi + \theta$$

While the thrust profiles for the different technologies vary, the overall PowerSail trajectory is similar in all cases. It represents a hybrid motion between the sun pointing and minimum aero solutions presented in Section 4. By exploiting the trade-off between pointing accuracy and fuel mass, the hybrid trajectory requires less mass than the true sun pointing or the true minimum aero solutions.

Table 5-1 summarizes the key mass optimal results. It is interesting to note that the PowerSail size converged to approximately the same value, independent of thruster technology. This can be explained by the tendency of the solution to favor small, and thus light, PowerSails. In all cases the pointing accuracy was allowed to slip up to the maximum allowable error in power generation, or 1468 MJ (5%).

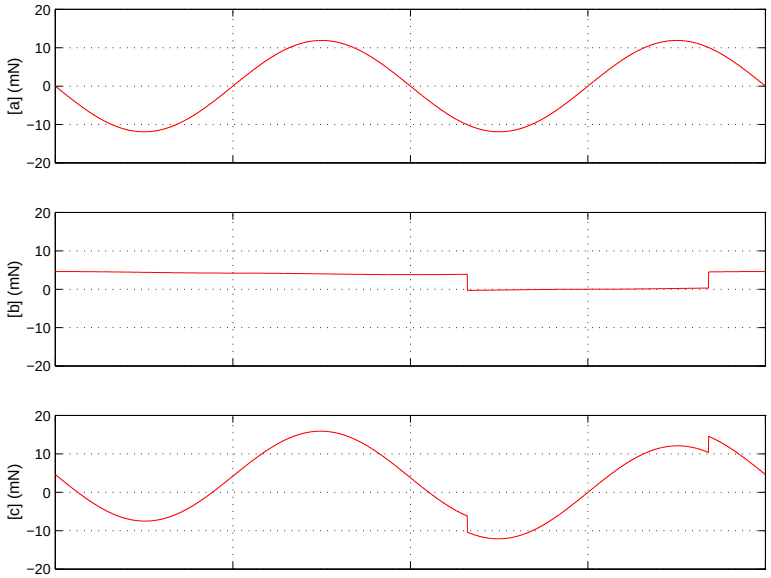

Figure 5-1: Decomposition of the throttle-able force F_{y1} (see the blue line in Figure 4-5) into a component that generates a net PowerSail moment (a), a component that generates no moment (b), and the total force (c).

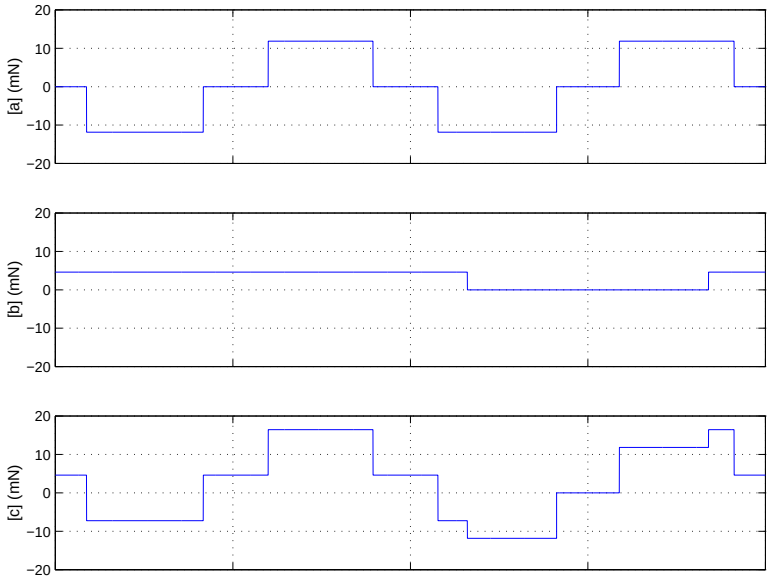

Figure 5-2: Decomposition of the approximate pulse force F_{y1} into a component that generates a net PowerSail moment (a), a component that generates only force (b), and the total force (c).

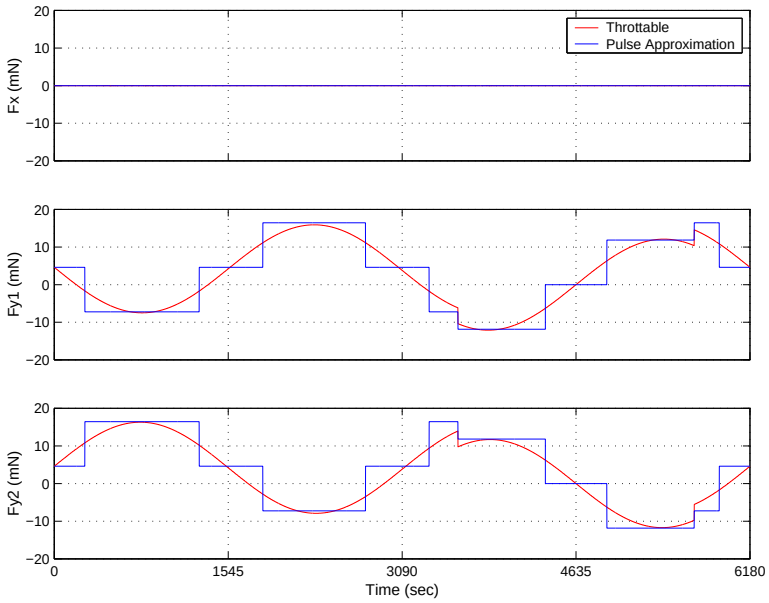

Figure 5-3: Comparison of an approximate pulse profile with the throttle-able solution that it is based on.

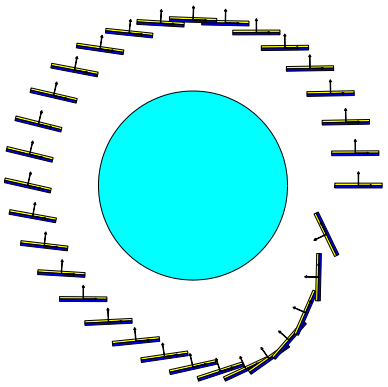

(a) trajectory

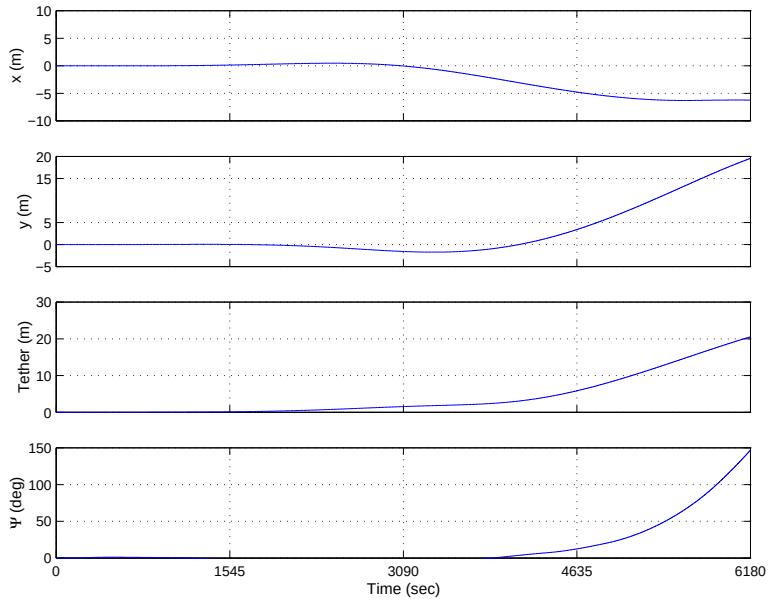

(b) x, y, tether length and inertial Ψ

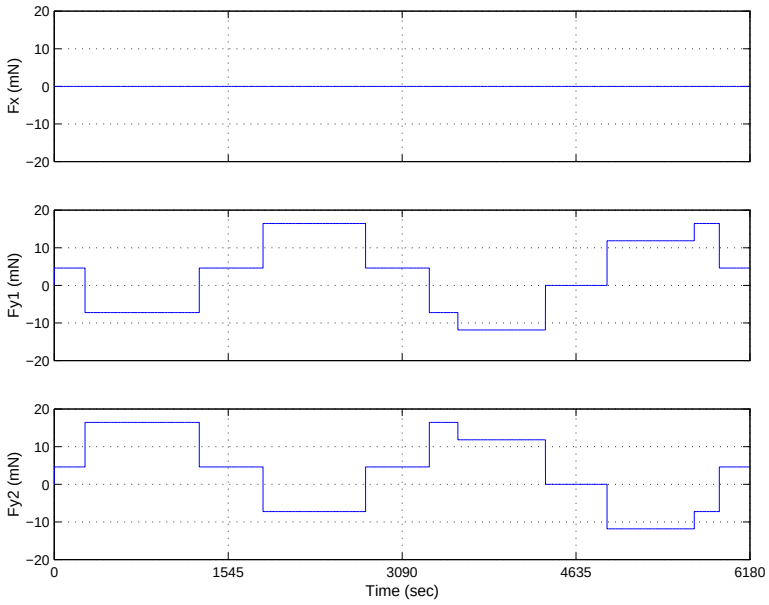

(c) thrust forces

Figure 5-4: Dynamic simulation results using the pulse approximation thrust profiles derived from the throttleable results.

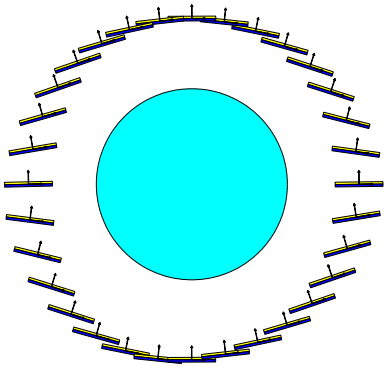

(a) trajectory

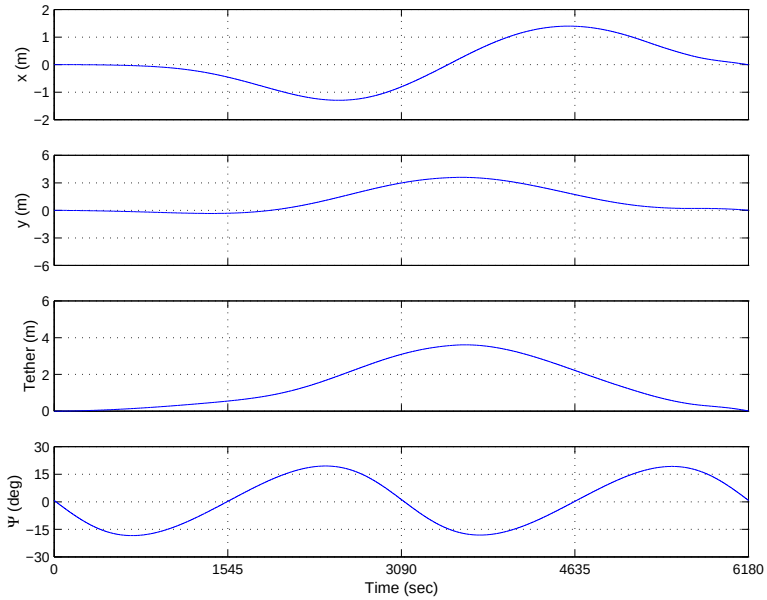

(b) x, y, tether length and inertial Ψ

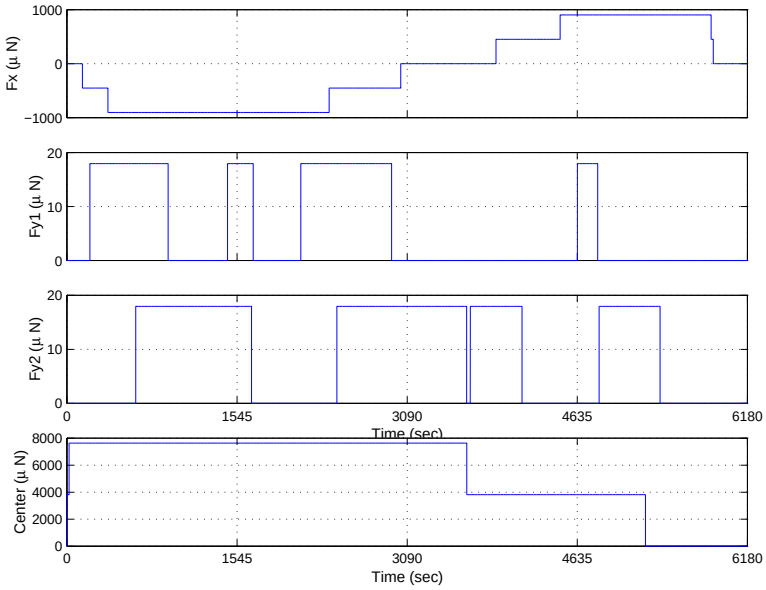

(c) thrust forces

Figure 5-5: Mass optimal results using teflon PPT thruster technology.

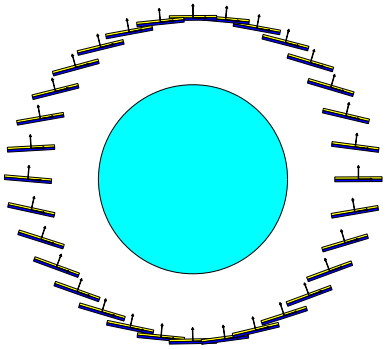

(a) trajectory

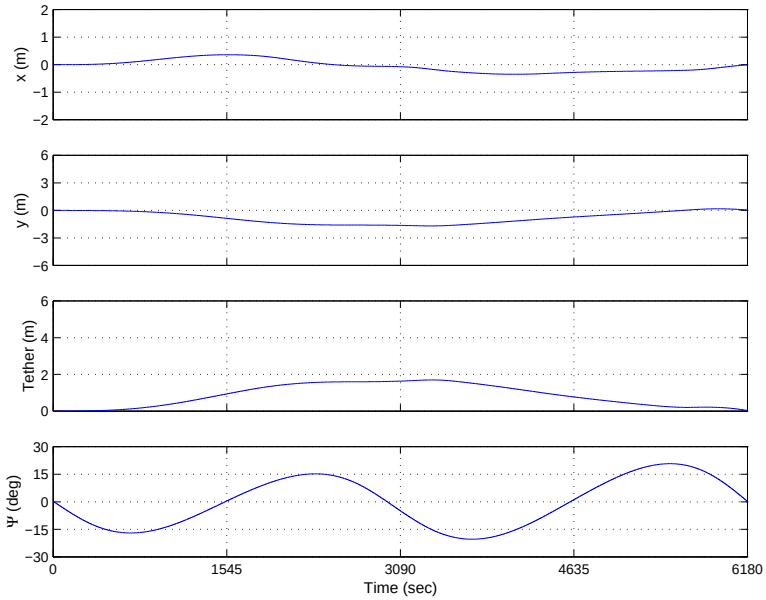

(b) x, y, tether length and inertial Ψ

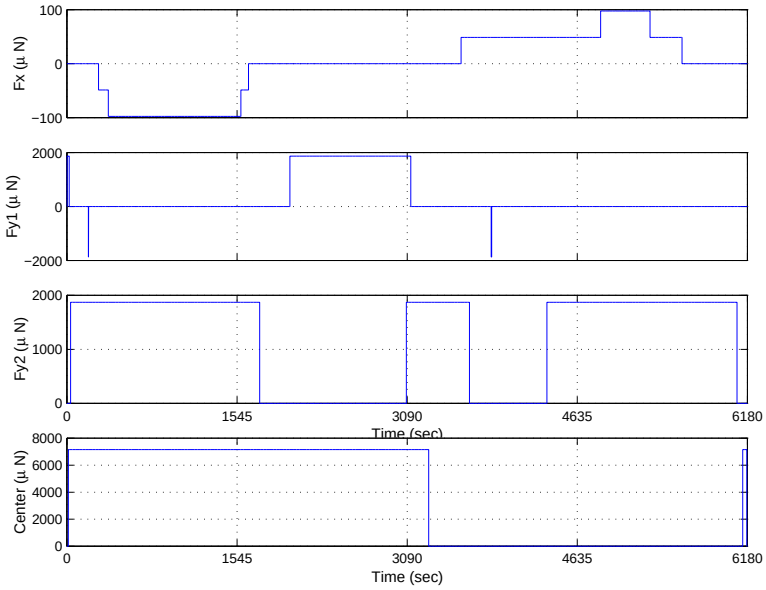

(c) thrust forces

Figure 5-6: Mass optimal results using hydrazine resistojet thruster technology.

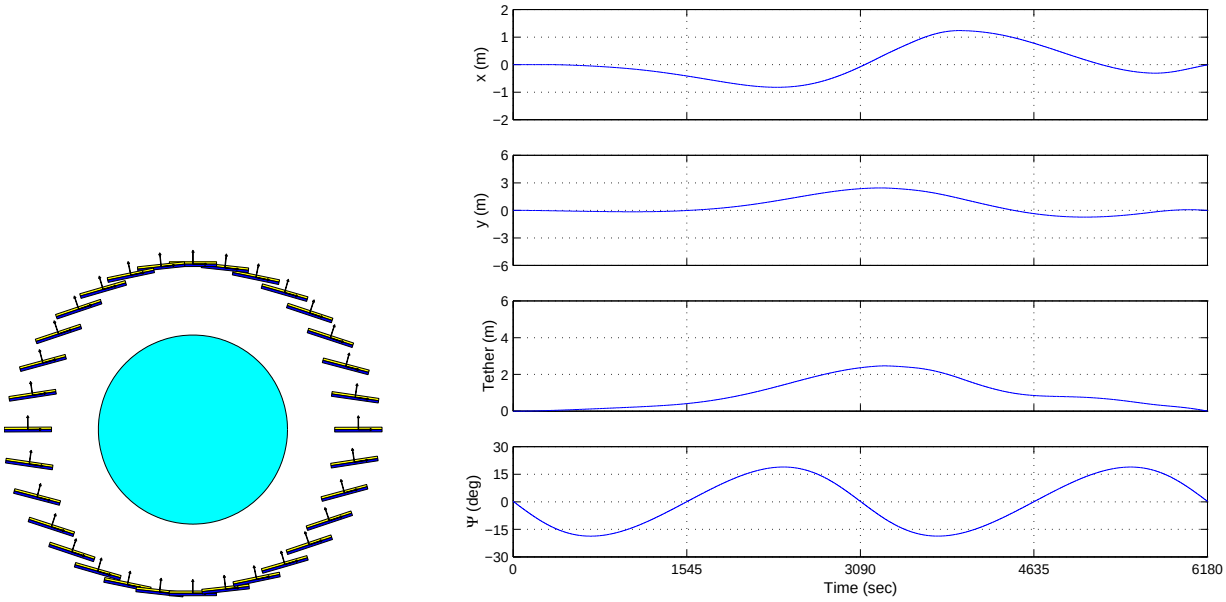

(a) trajectory

(b) x, y, tether length and inertial Ψ

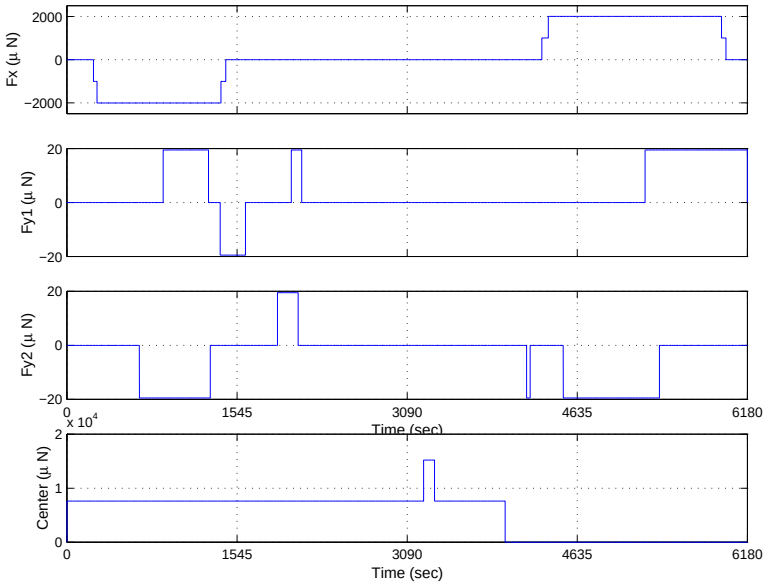

(c) thrust forces

Figure 5-7: Mass optimal results using hydrazine arcjet thruster technology.

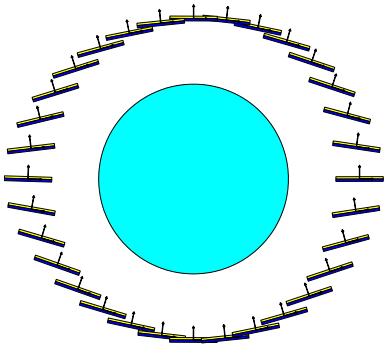

(a) trajectory

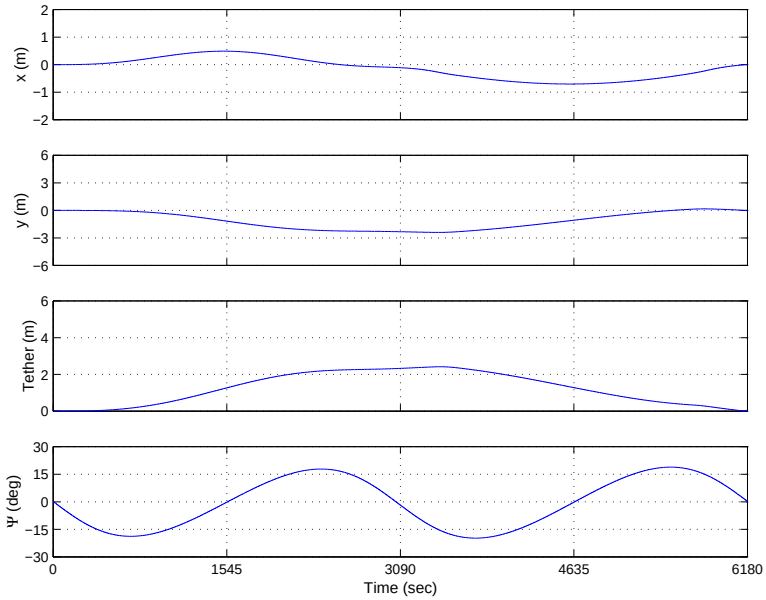

(b) x, y, tether length and inertial Ψ

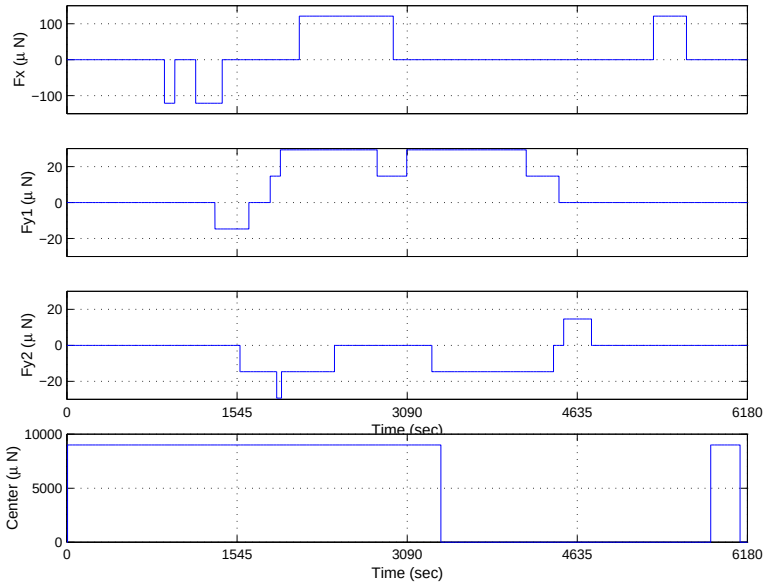

(c) thrust forces

Figure 5-8: Mass optimal results using ammonia arcjet thruster technology.

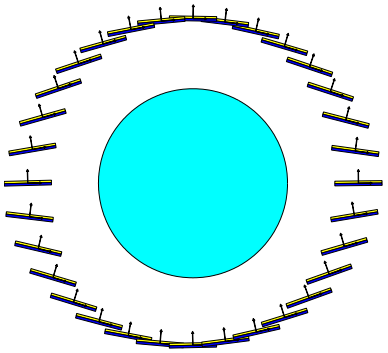

(a) trajectory

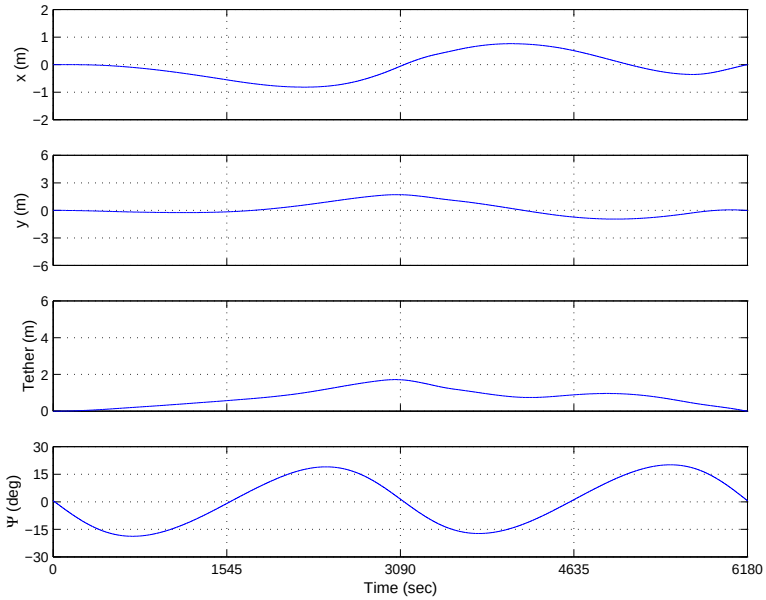

(b) x, y, tether length and inertial Ψ

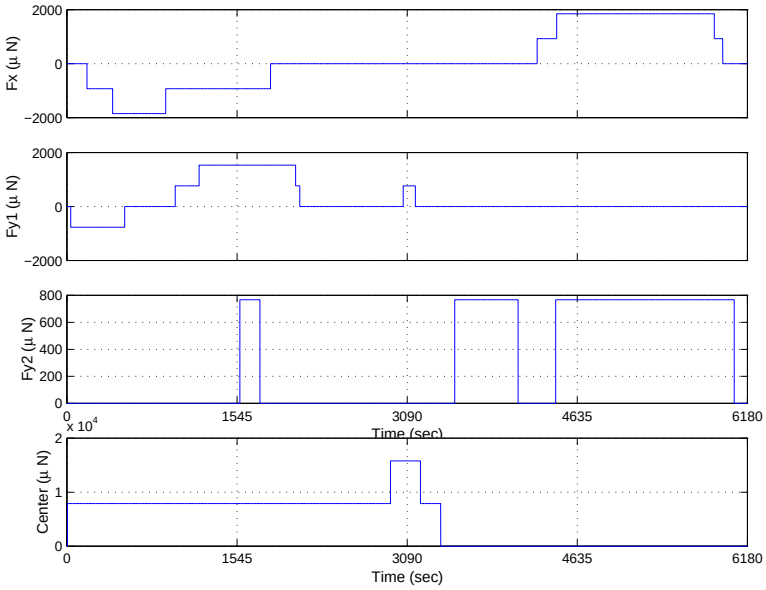

(c) thrust forces

Figure 5-9: Mass optimal results using hydrogen arcjet thruster technology.

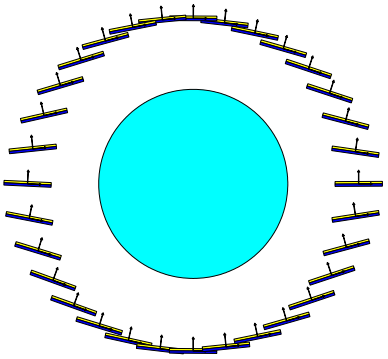

(a) trajectory

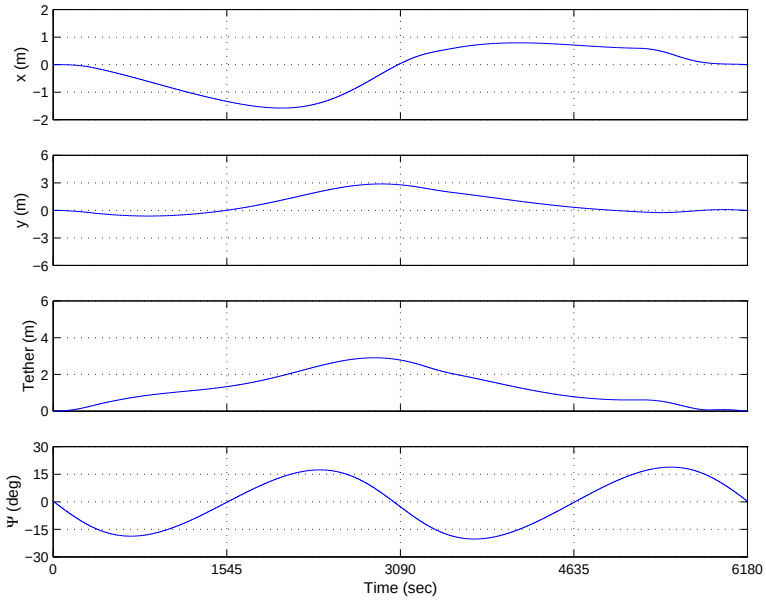

(b) x, y, tether length and inertial Ψ

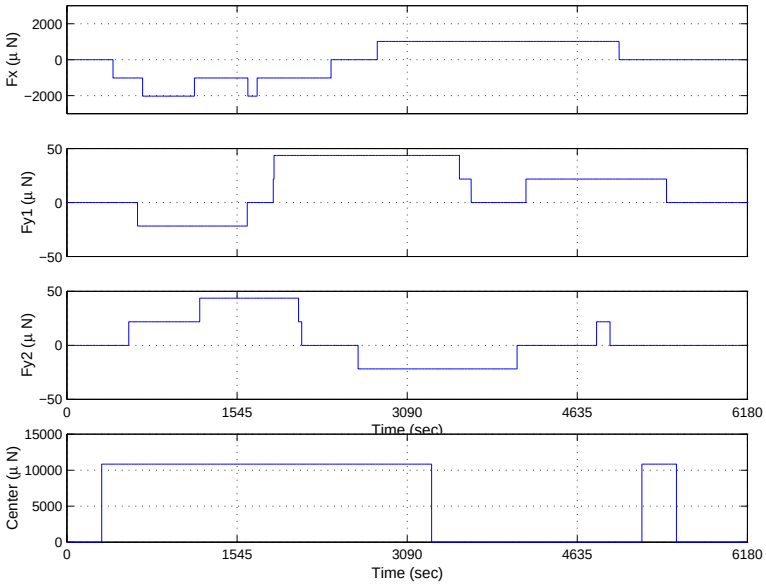

(c) thrust forces

Figure 5-10: Mass optimal results using xenon hall thruster technology.

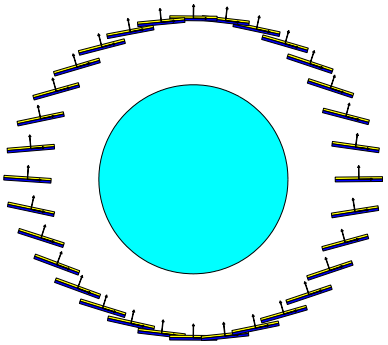

(a) trajectory

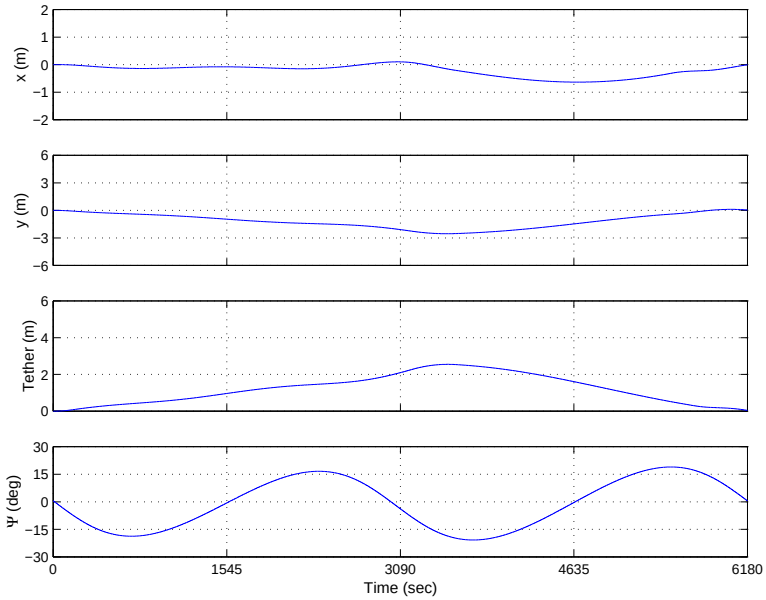

(b) x, y, tether length and inertial Ψ

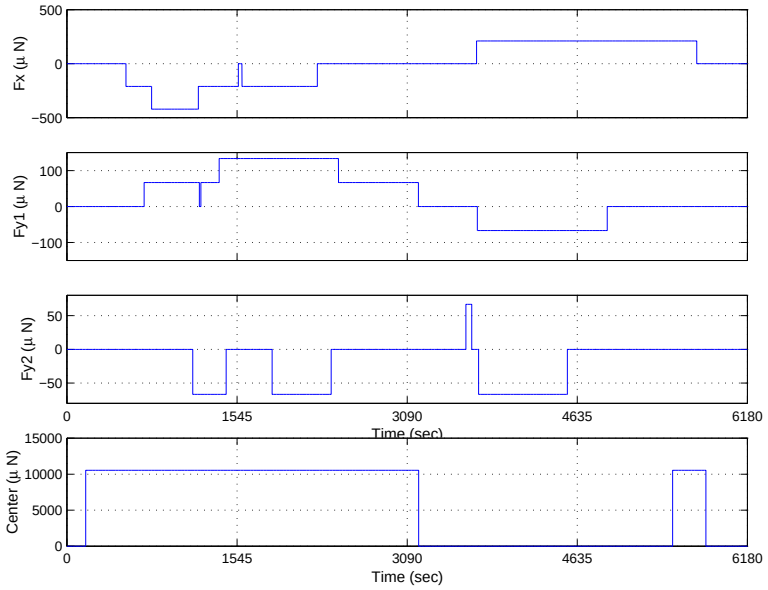

(c) thrust forces

Figure 5-11: Mass optimal results using xenon ion thruster technology.

6 Propulsion System Sizing Calculations

Based on the optimal dynamic simulation outlined in the previous section we can calculate the required propulsion system mass, power, and overall vehicle size for a given mission. In this section of the report we will discuss the vehicle characteristics for the various propulsion technologies considered.

6.1 Powersail Thruster Layout

The optimal thruster pulse generation profile constraints and assumptions were outlined previously in Section 5.2. These constraints can be interpreted in terms of thruster hardware and layout as detailed in Figure 6-1.

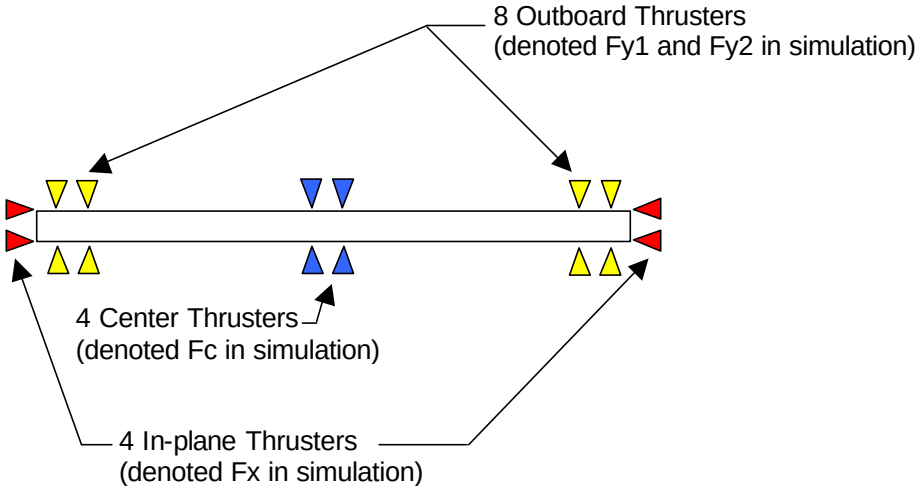

Figure 6-1. Schematic showing thruster layout implied by force constraints imposed in the dynamic simulation/optimization routine.

The total number of thruster units on the vehicle amounts to sixteen. Although all sixteen thrusters are assumed to be of the same type (e.g. N_2H_4 Arcjet, Xe Ion, etc.), a variation between groups has been allowed in the optimization routine. The thruster requirements and deviations can be summarized:

- The eight outboard thrusters all have the same thrust amplitude and, hence, power requirements
- The four center thrusters all have the same thrust amplitude and, hence, power requirements
- The four in-plane thrusters all have the same thrust amplitude and, hence, power requirements
- The on-board power processing system is capable of simultaneously firing all sixteen thrusters

6.2 Propulsion Mass and Power Analysis

The optimization algorithm determines the thrust amplitude for each set of thrusters (outboard, center, and in-plane) as well as the total firing duration for each thruster. This information can be used to calculate the mass contribution of the propulsion system to the overall vehicle. Since this study was limited to EP devices, the propulsion system mass, m_{sys}, can be written as

$$m_{sys} = m_{fuel} + m_{inert} \tag{90}$$

where m_{fuel} is the fuel mass and m_{inert} is the dry mass, which includes the PPU as well as the thruster unit itself.

With the thrust amplitude and total firing time given for each thruster, it is straightforward to calculate the total required per-orbit impulse, $\Sigma \hat{F}$. Knowing $\Sigma \hat{F}$ and the total number of orbits in the mission, n, the mission fuel mass is calculated as

$$m_{fuel} = \frac{n\Sigma\hat{F}}{gI_{sp}}. \tag{91}$$

The inert mass is assumed to scale proportionately with the required electrical power, or

$$m_{inert} = bP \tag{92}$$

where P is the electrical power demanded of the thruster and the constant of proportionality, b, has units of kg/kW. The inert mass has contributions from both the power processing hardware as well as the thruster unit itself, so b can be broken down into

$$b = b_{PPU} + b_T. \tag{93}$$

Electrical power can be related to the thrust amplitude through a fundamental relationship according to

$$P = \frac{FgI_{sp}}{h} \tag{94}$$

where F is the thrust amplitude and η is the electrical efficiency of the propulsion system. With this expression we can write the inert mass in terms of the thrust

$$m_{inert} = \frac{bFgI_{sp}}{h} \; ? \tag{95}$$

Thus, when the optimization routine specifies the thrust amplitude it is implicitly fixing the thruster power as well as the required inert mass for a given thruster technology.

To calculate the total propulsion system mass contribution we must slightly modify the inert mass expression to take into account the three sets of thrusters: outboard, center, and in-plane. Since there are eight identical outboard thrusters, the inert mass due to the outboard thrusters can be written as

$$m_{inert,out} = \frac{8bF_{out}gI_{sp}}{h}. \tag{96}$$

Similar expressions can be written for the four center thrusters and the four in-plane thrusters. Finally, the total propulsion system mass is given:

$$m_{sys} = \frac{n\Sigma\hat{F}}{gI_{sp}} + \left(8F_{out} + 4F_{in} + 4F_{center}\right)\frac{bgI_{sp}}{h}. \tag{97}$$

6.3 Vehicle Performance Summary

The input parameters to the optimizer algorithm were

- Orbital period = 6180 sec
- Orbit radius = 7,277,759 m
- Sail structure areal density = 0.92 kg/m^2
- Sail vehicle aspect ratio = 1:1
- Solar energy produced per orbit must be within 5% of 1.545 x 10^9 J
- Solar cell efficiency = 15%
- Power-specific mass of PPU = β_{PPU} kg/kW
- Power-specific mass of thruster unit = β_T kg/kW
- Thruster power efficiency = η
- Thruster specific impulse = I_{sp} sec

Based on these parameters and previously discussed constraints, the optimizer was free to choose

- Thrust amplitude for eight outboard thrusters
- Thrust amplitude for four center thrusters
- Thrust amplitude for four in-plane thrusters
- Thruster firing profile (subject to pulse constraints discussed in Section 5-2)
- Physical size of sail array (subject to 1:1 aspect ratio requirement)

with the goal of minimizing the total vehicle mass for the given solar energy generation requirement.

Seven different thruster technologies were investigated. The resulting trajectory analyses were presented earlier in Figures 5-5 through 5-11. The corresponding propulsion system implications and overall vehicle performance are summarized in Table 6-1. A plot comparing the overall vehicle mass for the seven technologies is included as Figure 6-2.

	Teflon PPT	N2H4 Resistojet	N2H4 Arcjet	NH3 Arcjet	H2 Arcjet	Xe Hall	Xe Ion
Isp (sec)	1000	300	500	600	1000	1600	3000
β Thruster (kg/W)	1.2E-01	2.0E-03	7.0E-04	7.0E-04	5.0E-04	3.0E-03	6.0E-03
β PPU (kg/W)	1.1E-01	1.0E-03	2.5E-03	3.0E-03	2.5E-03	1.0E-02	1.0E-02
Efficiency	0.07	0.80	0.35	0.36	0.40	0.50	0.65
Number of Thrusters	16	16	16	16	16	16	16
Total Impulse per Orbit (N-s)	37.64	33.53	36.67	33.22	37.59	40.91	36.32
Number of orbits	51030	51030	51030	51030	51030	51030	51030
Center Thrust Amp. (N)	3.81E-03	7.16E-03	7.60E-03	9.01E-03	7.89E-03	1.08E-02	1.05E-02
Outboard Thrust Amp. (N)	1.80E-05	1.87E-03	1.95E-05	1.46E-05	7.67E-04	2.18E-05	6.67E-05
In-Plane Thrust Amp. (N)	4.52E-04	4.88E-05	1.00E-03	1.21E-04	9.25E-04	1.01E-04	2.10E-04
Center Thruster Power (W)	534.5	26.3	106.6	147.2	193.6	340.4	476.9
Outboard Thruster Power (W)	2.5	6.9	0.3	0.2	18.8	0.7	3.0
In-Plane Thruster Power (W)	63.4	0.2	14.1	2.0	22.7	3.2	9.5
Fuel Mass (kg)	195.8	581.4	381.5	288.0	195.5	133.0	63.0
Inert (PPU+Thruster) Mass (kg)	554.7	0.5	1.6	2.2	3.0	17.9	31.5
Sail Mass (kg)	1616.4	1609.6	1616	1615	1616.3	1615.5	1614.1
Total Vehicle Mass (kg)	2366.9	2191.5	1999.1	1905.2	1814.9	1766.4	1708.6
Sail Edge Length (m)	41.92	41.83	41.91	41.9	41.92	41.89	41.89
Max Formation Error (m)	3.6	1.6	2.4	2.5	1.7	2.9	2.7

Table 6-1. Summary of optimizer results for seven different thruster technologies. Data here reflect the trajectories previously presented in Figures 5-5 through 5-11.

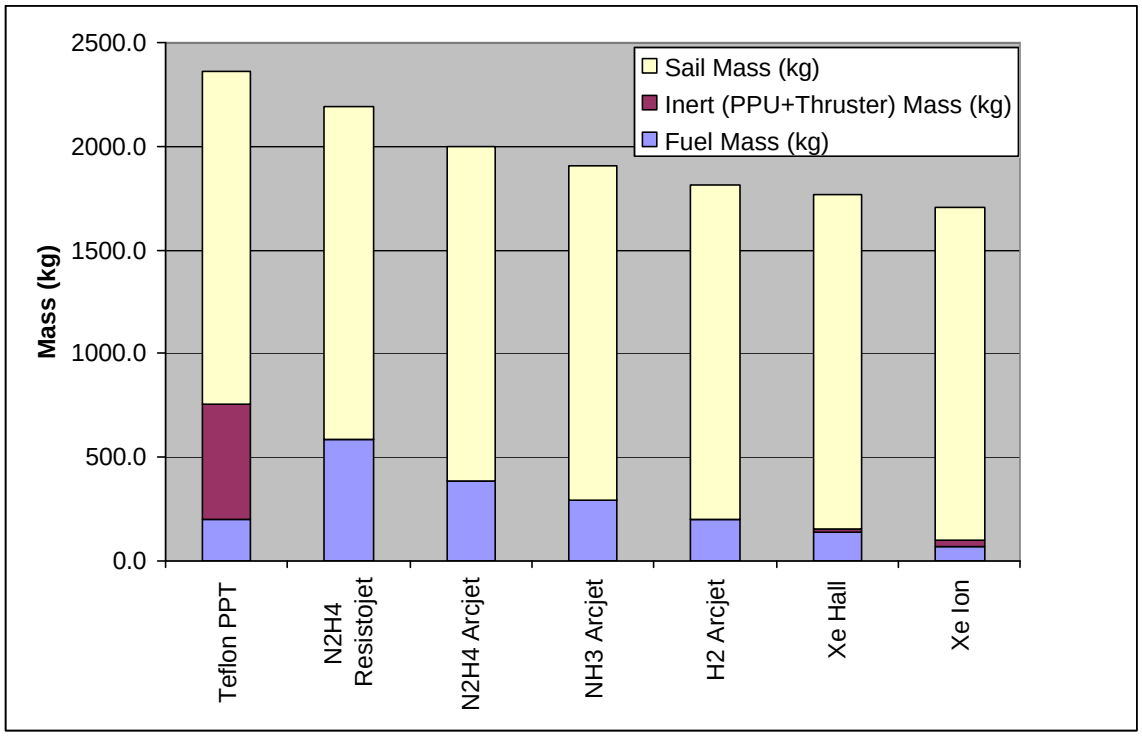

Figure 6-2. Comparison of total vehicle mass for optimized trajectories.

7 Closing Remarks

7.1 Summary

The goal of this work was to investigate practical vehicle sizing and performance requirements for a free-flying 500-kW solar array in orbital formation with a power-consuming host vehicle. To meet these requirements, the sail vehicle must employ propulsion for two functions: formation-keeping with host and ACS/Sun-pointing maneuvers. The equations of motion were developed assuming a rigid vehicle subject to gravity, aerodynamic drag, and solar pressure.

For preliminary analyses, investigators calculated the required sail size (mass), and force profiles for three pre-defined orbital trajectories: 1) Minimum aerodynamic drag; 2) Minimum gravity gradient torque; and 3) Direct sun-pointing. In this analysis, the thrusters were assumed to have unrealistic throttleability and formation-flying constraints. The performance characteristics of a 1,000-sec-I_{sp} thruster were assumed as a candidate technology. Results indicated the best performance (lowest vehicle mass) for the direct sun-pointing trajectory, with the minimum gravity-gradient torque as the most massive vehicle. The per-orbit impulse requirements spanned 50 to 98 N-s for the three trajectories studied.

The trajectory study brought to light a design trade-space involving the overall vehicle dimensions (area) and required thruster mass. The trade-space involved balancing propulsion resources with required solar

energy absorbed per-orbit. The trade is defined by competing effects concerning array sun pointing: 1) if the array normal is allowed to slip from true sun pointing then the propulsion system mass required for attitude control can be reduced; 2) if the array sun-pointing angle deviates from normal, then a larger (more massive) array area will be necessary to collect the required solar energy per-orbit. Based on the competing mass effects an optimal trajectory was pursued. The optimal trajectory depends upon thruster technology, as some thrusters will impose a greater mass expense in order to save a given amount of array area (mass) through attitude control.

Performance characteristics of real EP thrusters necessitated a different approach from the preliminary analysis. Although a generalization, it is prudent to assume that EP thrusters are not throttleable. Thruster hardware is usually designed and optimized for a single performance point (e.g. thrust amplitude, specific impulse) or a narrow range about a fixed point. Thus, the continuously throttleable solution from the preliminary analysis becomes a somewhat unrealistic starting point. Lessons learned from the preliminary analysis were used to estimate realistic EP thrust profiles, employing discrete thrust amplitude pulses, with the goal of achieving desired flight trajectories. It soon became apparent that the relation between the overall vehicle trajectory and the thruster pulse profile was non-intuitive.

A trajectory optimization algorithm and computer code were developed to explore the attitude control/formation-flying/thruster trade-space for realistic EP technologies. Based on defined orbit parameters, formation constraints, solar energy constraints, and thruster limitations, the optimization routine was capable of calculating the required sail size and mass, thrust amplitude, and thruster firing profile such that the overall vehicle mass was an extremum. The vehicle was configured with eight out-board (moment-producing) thrusters, four center (no moment) thrusters, and four in-plane thrusters of the same technology, but different thrust amplitude. The tool was used to compute the trajectories and associated vehicle sizing parameters for seven canonical EP thruster technologies. The lowest vehicle mass was found to be 1,708 kg for a 41.89-meter square array propelled using xenon ion thrusters in a near-sun-pointing trajectory, with the PPT being the worst performer with a vehicle mass of 2,367 kg.

7.2 Conclusions

Although only an exploratory study, the results of this work yield the following conclusions.

- The optimized trajectory found significant propulsion mass savings over analytical design estimates. The optimization tool found a 60% savings on required per-orbit impulse for a hydrogen arcjet when compared with the 1,000-sec-I_{sp} canonical case, reflecting an overall vehicle mass savings of 11%.

- As propulsive flexibility is made more robust, the optimization tool will exploit the added degrees-of-freedom to provide greater mass savings. The configuration documented in this report, that of 16 thrusters distributed as prescribed, likely does not represent a hard minimum vehicle mass. Adding more thrusters, more pulsing repetitions, capability to mix technologies on the same vehicle, thrust vectoring, limited throttlability, etc. are likely to provide improved mass savings.

- Propulsion savings may be possible by relaxing the formation-flying constraint. As a starting point, the work reported here constrained the sail vehicle to have zero formation error after one orbit. Trajectories calculated according to this constraint displayed a formation position error less than five meters during the orbit for all cases.

- The imposed limitation requiring identical thruster technology was overly restrictive. Examination of the optimized results indicated that the majority of the propulsive work was carried by the center thruster package, while the out-board ACS thrusters were least utilized. As such, the optimized results implied the use of unrealistic technology, such as 700-mW Hall thrusters or 500-W PPT's.

- Although not studied quantitatively, results indicate that an attractive vehicle design could consist of a Hall or ion thruster for the center package, coupled with a PPT as an out-board technology. Such a configuration may be advantageous from a vehicle deployment standpoint: the center of the sail, which will likely consist of the spacecraft bus, can house the xenon technologies and incorporate propellant storage and flow control devices, while the out-board PPT's would require only electrical connection. This would make in-space deployment of the stowed vehicle practical and avoid complicated propellant routing.

7.3 Suggestions for Future Work

Results of this preliminary design study naturally led to inspiration for follow-on studies. Aerophysics investigators make the following recommendations for future work.

- At the expense of computation time, an optimization tool could be modified to explore a number of different vehicle configurations with increased flexibility. Specifically, it is recommended to investigate the effects of mixed propulsion technologies on the same vehicle, limited throttleability consistent with thruster state-of-the-art, and limited thrust vectorability. It is reasonable to assume that vehicle mass reductions will arise from such studies.

- The analyses here were performed for a single canonical orbit: 900-km circular in-plane with the sun pointing vector. It is imperative to explore the behavior of different orbital regimes. For instance, as the altitude decreases the affect of atmospheric drag will become more pronounced as will the magnitude of gravity-gradient torque. The resulting optimal trajectory and propulsive needs will differ as the vehicle must counter different perturbations. Likewise, higher orbits and different inclinations will impact vehicle sizing.

- Flexible vehicle dynamics need to be incorporated into the equations of motion. Distributed mass and modal behavior will influence required per-orbit impulse as well as optimal thrust amplitudes and pulse firing history. The effects of spacecraft flexibility are not readily intuitive.